2020-01-01

Relating Surface Resistivity To Corrosion Of Rebar Embedded In Portland Cement Concrete

Luisa Alejandra Morales
University of Texas at El Paso

RELATING SURFACE RESISTIVITY TO CORROSION OF REBAR EMBEDDED IN PORTLAND CEMENT CONCRETE

LUISA ALEJANDRA MORALES

Master´s Program in Civil Engineering

APPROVED:

Soheil Nazarian, PhD., Chair

Arturo Bronson, PhD.

Danniel Rodriguez, PhD.

Stephen L. Crites, Jr., Ph.D.
Dean of the Graduate School

RELATING SURFACE RESISTIVITY TO CORROSION OF REBAR EMBEDDED IN PORTLAND CEMENT CONCRETE

by

LUISA A. MORALES, BSCE

THESIS

Presented to the Faculty of the Graduate School of

The University of Texas at El Paso

in Partial Fulfillment

of the Requirements

for the Degree of

MASTER OF SCIENCE

Department of Civil Engineering

THE UNIVERSITY OF TEXAS AT EL PASO

August 2020

Acknowledgements

There are several of people I would like to thank. First is my sincerest and warmest thank to Dr. Nazarian for his guidance, support, patience, opportunities, and for giving me the chance to work on this investigation. I would like to thank Dr. Bronson for all the advice and help throughout the years and mainly for introducing me into this topic. I would like to extend my gratitude to Dr. Rodriguez, Sergio Rocha and Jose Garibay for their valuable advice and help throughout the project.

I would like to thank the sponsors of this research project, Center for Transportation Infrastructure Systems (CTIS) at the University of Texas at El Paso and the Nuclear Regulatory Commission (NRC). I would like to recognize my colleagues, Sebastian Morales and Benjamin Arras, for all their help with laboratory work and their kindness.

I am extremely grateful to my parents, grandparents, brothers and sister for their full support, encouragement and belief in me. This is dedicated to all of you.

Abstract

Reinforced concrete is widely used as a construction material known for its durability and proficiency of withstanding large forces in severe environments. Despite that the majority of these structures result in long-term performance, there is still a large number of failures of reinforced concrete structures as a result in corrosion of the reinforcement and concrete degradation. It is critical to assess the state of the corroded structure to decide on whether maintaining or replacing the structure is needed. The objective of this study is to characterize a relationship between the steel reinforcement corrosion and the concrete's resistivity. It is widely accepted that the corrosion rate increases with decreasing concrete resistivity under common environmental exposure conditions except of those structures submerged in water. To evaluate the corrosion measurements of the reinforcement, Linear Polarization Resistance and Tafel were used to assess the accelerated tests with a current supply coupled with the concrete's surface resistivity. The research work presented in this thesis was performed on Portland cement carbon steel reinforced concrete specimens under accelerated testing exposed to different environment conditions and concrete mixes.

Table of Contents

List of Tables

List of Figures

Chapter 1. Introduction

1.1 Problem Statement

Reinforced concrete structures are widely used in construction because of its durability, toughness, and cost. The corrosion of carbon steel bars that are commonly used in reinforced concrete is usually of concern since it may compromise the integrity of the structure. The estimated annual cost of maintaining or replacing damaged bridges due to corrosion in 2003 was $8.3 billion (Fakhri, 2019). It is critical to assess the structure's state of corrosion in order to decide on whether maintaining or replacing it with a new structure.

The steel corrosion initiates when the concrete is exposed to a moist environment. Corrosion rate depends on the resistivity of the concrete, and the exposure conditions such as moisture, temperature, oxygen ions, and chloride ions. Cracks in concrete act as pathways for the penetration of corrosion agents of the outside environment and accelerate the corrosion process. A completely dry environment with no moisture will cause no corrosion to the rebar. A passivation film is formed around the carbon steel rebar by the high alkalinity of the concrete and creates minor cracks on the concrete (Figueira, 2016). Moisture from precipitation can penetrate through the voids and cracks of the concrete and can react with the carbon steel and generate rust. The formation of rust causes delamination or deformation of the concrete since the volume of the rust is much greater than that the steel and expands against the concrete.

The rate of corrosion is typically estimated indirectly from nondestructive or semi-destructive techniques such as the electrical resistivity (ER), half-cell potential (HCP), or galvanostatic pulse measurement (GPM). The Electrical Resistivity technique applies a current to the surface of concrete to measure the voltage and calculate its resistivity. The higher the resistivity is, the lower the potential for corrosion rate will be. More advanced electrochemical techniques, such as the Linear Polarization Resistance (LPR) or Tafel extrapolation, are sometimes used to estimate more

accurately the corrosion rate of the reinforcement. The LPR and Tafel techniques apply a current to the reinforced steel in order to estimate its corrosion rate of steel through the flow of electron loss. A strong relationship between the concrete's electric properties with the reinforcement's corrosion is fundamental to predict the service life of a reinforced concrete structure.

1.2 Objectives

The main goal of this study is to establish the interrelationship among the results of LPR, Tafel and Electrical Resistivity of reinforced concrete under different environment conditions and concrete mixes. In order to achieve that goal, the following objectives were fulfilled:

1. To formulate an approach to simulate the corrosion of rebars embedded in concrete realistically and in an accelerated fashion under different environmental conditions.
2. To determine the versatility of LPR and Tafel techniques in estimating the corrosion of the reinforcement.
3. To correlate the concrete's resistivity to the reinforcement's corrosion rate.

In achieve those objectives, several reinforced concrete specimens were prepared and subjected to simulated atmospheric moisture, marine environment and less saline submerged condition. The LPR and Tafel methods were employed to monitor the corrosion of carbon steel rebars and the Electrical Resistivity method was used to measure the resistivity of reinforced concrete beams under the three environmental conditions.

1.3 Organization

The study on accelerated corrosion testing of reinforced concrete is structured into five chapters. Chapter 1 is the introductory chapter with a brief characterization and background of

corrosion in reinforced concrete and addresses the objectives of this study. Chapter 2 is an extensive literature review of corrosion study in reinforced concrete. Chapter 3 is a review on the instrumentation and materials used for this accelerated corrosion study. This chapter also consists of the test concept and the experimental approach conducted to monitor the corrosion of the simulated accelerated testing of the reinforce concrete. The results obtained in this study are shown in Chapter 4, used to investigate the corrosion rate and resistivity of the reinforced concrete. Chapter 5 summarizes the conclusions and contributions of other corrosion related studies. This chapter also covers recommendations for future research of the study.

Chapter 2. Literature Review

Corrosion of carbon steel is one of the main causes of degradation of reinforced concrete structures. The passivation layer of the carbon steel is formed by the alkalinity content and consequently ruptured by the carbon dioxide content of the concrete. The curing period of the concrete generate strains and tensions that might cause formation of cracks, reducing the efficiency of the concrete and allowing the ingress of corrosion agents (Figueira, 2016). This chapter goes further into detail on the definition of corrosion and main factors that contribute to the mechanism of corrosion.

2.1 Corrosion of Steel in Concrete

Corrosion is the loss of metal caused by oxidation that creates a cathode area and an anode area in the reinforcement. Increasing the temperature will accelerate the corrosion rate. Chloride ions and carbon dioxide ions are other factors that induce corrosion (Figueira, 2016). The corrosion rate at which the steel bar rusts vary based on the location of the structure. For example, the rate of corrosion in a coastal area is greater than the corrosion rate in an arid area.

The presence of an electrolyte promotes both anodic and cathodic reactions in the same metal. The corrosion process is an electrochemical process can be explained by Equations 2.1 through 2.3 (Böhni, 2005):

$$2Fe \rightarrow 2Fe^{2+} + 4e^{-} \quad (2.1)$$

$$O_2 + 2H_2O + 4e^{-} \rightarrow 4OH^{-} \quad (2.2)$$

$$2Fe + 2H_2O + O_2 \rightarrow 2Fe(OH)_2 \quad (2.3)$$

Equation 2.1 explains the anodic reaction that promotes the dissolution of the metal, while Equation 2.2 explains the cathodic reaction that consumes the electrons released by the anodic

reaction. The flux of ions and electrons can be used to measure the corrosion rate of the metal, given as mass loss per unit of time and area. Equation 2.3 is the summation of the anodic and cathodic reactions to form a precipitate of ferrous hydroxide ($Fe(OH)_2$) that is further oxidized to form rust.

The corrosion of rebar can occur in two different forms, pitting corrosion and uniform corrosion (Figueira, 2016).Chloride attack mostly results in pitting corrosion that are randomly distributed along the rebar. Carbonation induced corrosion mostly results in a uniform corrosion in the form of a reduction of the cross-section of the rebar.

Figure 2.1 lists the four factors that contribute to the corrosion of rebars in reinforced concrete: oxygen, electrolyte concrete, carbonation (pH), and chloride, while Table 2.1 lists the four conditions that contributes to the initiation and progression of corrosion (Böhni, 2005). The first stage is the initiation phase of corrosion where the passive layer is broken, leading to the final stage of an electrolyte conducting the flux of electrons when an anodic and cathodic reaction exists.

2.2 Phases of Corrosion

Steel embedded in a concrete with high alkalinity (pH greater than 12.5) is well protected from corrosion due to the formation of a passive film (Böhni, 2005). However, the passive film can be ruptured by the presence of chloride ions of carbonation of concrete. The service life of reinforced concrete is defined in two corrosion phases, the initiation phase and the propagation phase (Tuutti, 1982). The initiation phase begins when the reinforcement's passive film is damaged by chloride attack or carbonation of the concrete. The initiation period depends on the penetration rate of the corrosive agent controlled by the chloride or carbonation content, depth of passive film, and quality of concrete. As the initiation phase ends, the propagation phase begins where corrosion continues following the cracking or spalling of concrete. The reinforcement

begins to build up rust generating tensile strain on the concrete. The cracks propagate until it reaches the outer surface of the concrete.

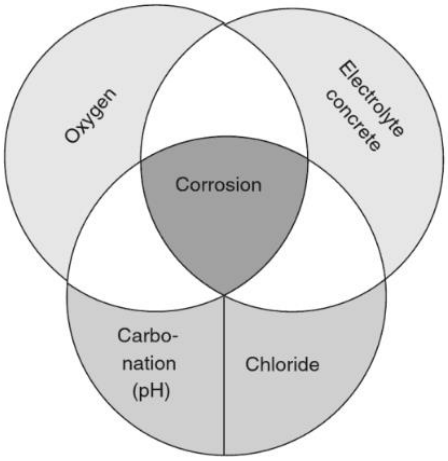

Figure 2.1 Four Factors Necessary to Induce Corrosion on Reinforced Concrete (Böhni, 2005).

Table 2.1 Conditions for *C*orrosion of Reinforced Concrete (Böhni, 2005)

Condition for Corrosion of Steel in Concrete	Condition is fulfilled, if:
An anodic reaction is possible	The passive layer of the steel bar breaks down and depassivation of the steel occurs. This can be caused by carbonation of concrete (lowering the pH of the pore water) and ingress of chloride into the concrete, reaching a critical level.
A cathodic reaction is possible	Oxygen as the driving force of the corrosion process is available at the interface of the reinforcement in a reasonable amount.
A flux of ions between the site of the anodic reaction and the site of the cathodic reaction is possible.	The environment or electrolyte between the site of the anodic reaction and the site of the cathodic reaction conducts well.
A flux of electrons is possible.	There is a metallic connection between the sites of anodic and cathodic reactions. For monolithic reinforced concrete structures this condition is usually fulfilled.

Two common models for assessing the service life of a concrete member are proposed by Tuutti (1982) and Liu and Weyers (1998). Tuutti (1982) modeled the service life of a concrete structure due to corrosion into an initiation stage and a propagation stage. The initiation period is controlled by the penetration and the concentration of the substances to the concrete cover and

finally to the reinforcing steel. Tuutti's results originated from several accelerated experiments of reinforced concrete done by applying voltage and different environmental conditions. To accelerate the corrosion of steel, two possibilities were established, applying voltage and admixing chlorides with drying and wetting cycles. The corrosion rate during the crack initiation period (T_0) is roughly zero in Tuutti's corrosion model (Figure 2.2). Tuutti's study estimated a propagation period (T_p) of 20 years for a reinforced concrete structure (Fakhri, 2019).

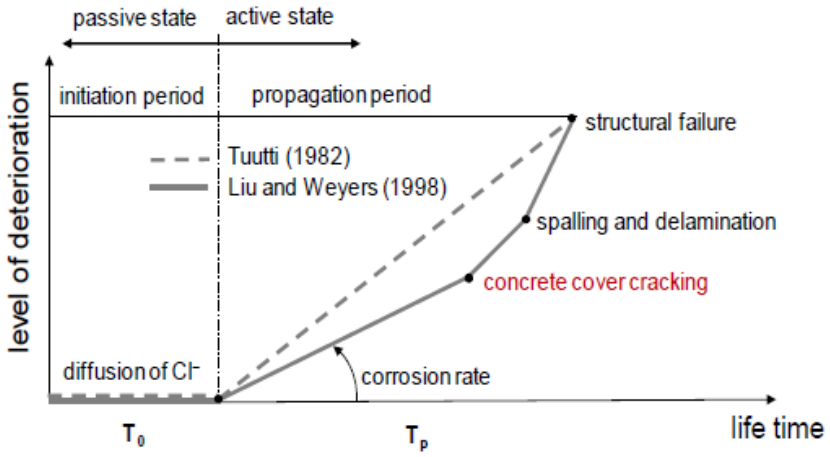

Figure 2.2 Reinforced Concrete Service Life Models (Fakhri, 2019)

Liu and Weyers (1998) developed a model that was more detailed than Tuutti's model based on accelerated experiments on reinforced concrete structures. Liu and Weyers investigated the effects of important variables such as the admixed chloride contents, concrete cover depths, reinforcing sizes and spacing, and exposure conditions. Three phases are shown in Liu and Weyers's deterioration model for predicting the remaining life: diffusion, corrosion, and deterioration. Diffusion is the phase where chloride ions penetrate the concrete. Corrosion is the propagation period from initial corrosion to first cracking of the concrete cover (about 2 to 5 years) (Liu and Weyers, 1988). Deterioration phase is the time for damage to consider repairing of the structure.

2.3 Carbonation Induced Corrosion

Carbonation induced corrosion is caused by the alkaline components of the cement paste with the carbon-dioxide ions from the environment (Figueira, 2016). This causes the pH of the concrete to decrease (become more acidic). Once the passivation film is ruptured by the carbonation or chloride ions, the rebar is exposed to corrosion. Corrosion due to carbonation depends on the depth of the carbonation in relation to the cover thickness as shown in the Table 2.2. Table 2.2 lists different carbonation depths of the concrete and the consequences that may lead to cracking and or spalling with relation to the corrosion condition.

Table 2.2 Carbonation Induced Corrosion (Parrot, 1994)

Depth of carbonation / cover thickness ratio	Concrete Condition	Rebar Condition	Risk of Corrosion
<0.5	No cracking	Passive	Negligible
>0.5	No cracking	Passive	Low
≈1.0	Small cracking	Low to moderate corrosion	High
>1.0	Cracks, minor detachment/spalling	Moderate to high corrosion	Very High
>>1.0	Cracks, high detachment/spalling	High corrosion with substantial loss of section	Very High/Severe

2.4 Chloride Induced Corrosion

Chloride induced corrosion occurs when chloride ions enter the concrete structure due to contamination of the raw materials, composition of the concrete mix with fine sands content, or by external sources such as de-icing salts and seawater (Figueira, 2016). Chloride ions decrease the pH and increase the conductivity of the reinforced concrete structure. The chloride-induced corrosion occurs in two phases. The corrosion initiation phase is the diffusion of the chloride ions

until it reaches the rebar's surface, and the propagation phase initiates when the chloride attacks the rebar followed by the cracking of the concrete member (Figueira, 2016).

The chloride threshold content, which is used for modeling the service life of reinforced concrete structures, is defined as the minimum chloride content relative to weight of cement that can initiate corrosion (Fakhri, 2019). Chloride content is associated with the weight of cement because it denotes the aggressive substance, Chloride (Cl^-), relative to the corrosion preventing substance, Hydroxide (OH^-). Two chloride thresholds are known: Chloride content for depassivation of steel surface, and chloride content that leads to deterioration. After depassivation, the threshold value is found to be a function of the moisture content and the quality of the concrete. Lower water cement ratio of the concrete results in higher threshold value. Table 2.3 lists references on similar investigations of accelerated corrosion testing in reinforced concrete using different technologies to access the service life of the concrete structure.

Table 2.3 Literature Review

Reference	Objective and Scope	Key Findings
Hornbostel et al. (2013)	To link the corrosion rate of reinforced concrete and concrete resistivity. Linear Polarization Resistance (LPR) was used to measure the corrosion rate.	Carbonation causes an increase in concrete resistance. The concrete resistivity can be different from the resistivity at the reinforcement. LPR measurements should be corrected for ohmic drop (when resistivity of concrete is too high).
Juhui and Cheung (2013)	A reinforced concrete bridge near the coastline was monitored to predict the chloride induce corrosion process using a finite element software. A model was proposed in this study to predict the cracks in concrete under different corrosion phases.	The proposed model predicts most of the experimental data where the depth between rebar and surface layer is less than 10 mm. This area is called the convection area because the chloride concentration if frequently changing. Cracks of the concrete were analyzed and concluded that the propagation of cracks in the concrete affect the corrosion rate readings of the reinforcement. In a chloride induced corrosion, the initiation time of the reinforcement corrosion is negligibly short.
Figueira (2016)	Reviews nondestructive methods (NDM) for corrosion monitoring of reinforced concrete structures done out in the field using electrochemical sensors. NDM such as open potential circuit, potentiostatic method, electric resistivity, noise analysis, and galvanic current were used to determine corrosion activity	NDMs allow quantifying the amount of metal that is corroded at a certain instant. Destructive methods give us indication of the average speed of corrosion. The use of NDM done with external sensors placed on the surface of the concrete are to be taken on the entire exterior surface of the concrete.
Loukil et al.(2016)	Accelerated tests were performed by applying a constant current to the concrete's reinforcement to study the cracks due to the corrosion of the steel reinforcement in concrete specimens.	The increase in the concrete resistance at the beginning of submersion is due to the development of resistive iron oxides forming a passivation layer around the rebar. The decrease in resistance is due to the concrete cracking and corrosion of the steel and concrete. Spots on the surface of the concrete do not reflect the internal corrosion state of the rebar.

Table 2.3 (cont.) Literature Review

Reference	Objective and Scope	Key Findings
Fattah et al. (2018)	Different mixtures of concrete were exposed to marine environment in three exposure regions; tidal, splash and atmospheric**.** Corrosion of concrete was assessed by conducting a chloride profiling and linear polarization resistance.	Based on measured chloride concentrations and resistivity values, fly ash and slag cement performed the best and Silica fume did not performed well.

Chapter 3. Instrumentation for Corrosion Investigation

3.1 Test Concept

As shown in Table 3.1, the materials typically used in the concrete mixture were Type I/II cement, dolomite limestone aggregates, fly-ash, and water reducer as developed by Wolf (2019).

Table 3.1 Aggregate Mix (Wolf, 2019)

Batch	Cement	Fly Ash	Water Reducer	Intermediate Agg.	Fine Agg.	w/c ratio
	%		oz./100 lbs. cement	%		
Small Agg.	80	20	10	60	40	0.45

The concrete specimens were mixed and poured in a mold similar to the one shown in Figure 3.1. The mold was retrofitted with four carbon steel rebars (top rebars in the figure) and four stainless steel rebars (bottom rebars) . The top and bottom rebars were spaced 4 in. apart, with the distance between the carbon steel and stainless steel rebars in each row of 2 in. To control the area of the rebar for corrosion testing, duct tape was taped around the reinforcement bar to preserve a nominal surface area of 34 cm^2.

The weight and length of the carbon steel rebars were recorded before pouring the concrete. As soon as practical after poring of the concrete, the specimen was transferred into a moisture room for 14 days of curing. On the second day of curing, the concrete specimens were demolded. Each specimen was then cut into four equal prisms with dimensions of 4 in. ×4 in. ×7 in. on the 14th day, as shown in Figure 3.2. The dimensions and weight of prism were also recorded.

Figure 3.1 Concrete Specimen Preparation

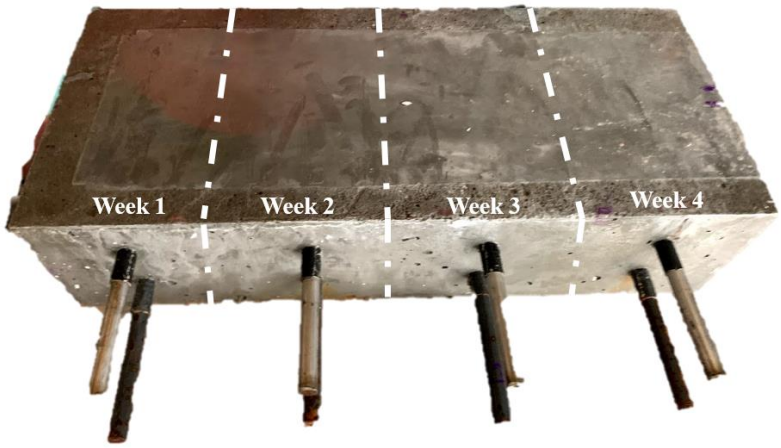

Figure 3.2 Concrete Specimen Assignation

To accelerate the corrosion process after 14 days of curing, the four prisms were connected to an electric current supply with a constant current of 20 mA for durations ranging from one week to four weeks. Each specimen was assigned a name corresponding to the duration that it was subjected to current. Week 1 prism (Figure 3.2) was connected for one week, Week 2 prism for 14 days, Week 3 prism for 21 days, and Week 4 prism for 28 days.

Starting from the pouring date, the resistivity of the four prisms was measured regularly. Since LPR testing is rapid and activated the surface significantly less than the Tafel tests, they were carried out in duplicate two to three days per week for four weeks on all prisms, leading to 24 LPR readings for each prism. For example, even though Week 1 prism was disconnected from the current after day 7, LPR tests were still performed for 28 days to assess the impact of the duration of applying current on the corrosion rate.

The Tafel tests activate electrochemically and change the metal surface, the tests were only carried out twice on each prism, one before connecting the prism to current and one after disconnecting from the current. For example, for Week 2 prism, a Tafel test was performed at day 1 and another at day 14. After 28 days, the carbon steel rebar embedded in each prism was carefully extracted, cleaned and weighed to quantify the mass loss due to corrosion

3.2 Experimental Design

The experiment design followed is shown in Table 3.2. Each set of experiments was developed to address a specific condition. For Set 1, three identical batches were made with the same concrete composition and each batch was subjected to corrosion under a different humidity. Mix 1 was set in an environmental chamber was set to a humidity of 90%, Mix 2 was submerged in a bucket of tap water with a conductivity of approximately 200 μF, and Mix 3 was set in a room with the humidity around 40%.

For Set 2, three identical batches were made with the same concrete composition and each batch was mixed with a different concentration of sodium-chloride to investigate the influence of the variation of chloride content inside the reinforced concrete. Mix 4, 5, and 6 were submerged in tap water.

Table 3.2 Test Concept Schedule

Set	Batch	Aggregate	Cement	$^{w}/_{c}$ ratio	Humidity %	NaCl %
1	1	Dolomite limestone	Type I/II	0.45	90	-
	2	Dolomite limestone	Type I/II	0.45	submerged	-
	3	Dolomite limestone	Type I/II	0.45	40	-
2	4	Dolomite limestone	Type I/II	0.45	submerged	0.8*
	5	Dolomite limestone	Type I/II	0.45	submerged	1.6*
	6	Dolomite limestone	Type I/II	0.45	submerged	2.4*
3	7	Dolomite limestone	Type I/II	0.4	submerged	-
	8	Dolomite limestone	Type I/II	0.4	submerged	3.5
	9	Dolomite limestone	Type I/II	0.5	submerged	-
	10	Dolomite limestone	Type I/II	0.5	submerged	3.5
4	11	Dolomite limestone	Type I/II	0.45	submerged	-
	12	Dolomite limestone	Type I/II	0.45	submerged	3.5
	13	Dolomite limestone	Type I/II	0.45	submerged	10.5
5	14	Dolomite limestone	Type V	0.45	submerged	-
	15	Dolomite limestone	Type V	0.45	submerged	3.5
	16	gravel	Type I/II	0.45	submerged	-
	17	gravel	Type I/II	0.45	submerged	3.5

* Added to the mix

For Set 3, two identical batches were made with the same concrete composition (Mix 7 and 8) with water-cement ratio of 0.4 and two additional batches with a water cement ratio of 0.5 (Mix 9 and 10). One batch of 0.4 water-cement ratio was submerged in tap water, and the other batch of 0.4 water-cement ratio was submerged in a 3.5% sodium chloride solution. A chloride concentration of 3.5% was designated to represent the salt content in a marine environment. One batch of 0.5 water-cement ratio was also submerged in tap water, and the other batch was submerged in a 3.5% sodium chloride solution.

For Set 4, three identical batches (Mix 11, 12 and 13) were made with the same concrete composition and each batch was submerged in tap water, 3.5% sodium chloride solution, and

10.5% sodium chloride solution to investigate the influence of chloride ingression in the reinforced concrete.

For Set 5, two identical batches were made with the same concrete composition (Mix 14 and 15) with Type V cement. Two additional batches of specimens used gravel as coarse aggregate (Mix 16 and 17) to assess the role of aggregate type. One batch of specimens with Type V cement was submerged in tap water, and the other batch was submerged in a 3. % sodium chloride solution. One batch of gravel mix was submerged in tap water, and the other batch of gravel was submerged in a 3.5% sodium chloride solution.

3.3 Testing Protocols

In this section the simulated accelerated corroding of the rebars and the tests conducted to monitor corrosion are presented.

Accelerated Corrosion of Rebars

Figure 3.3 demonstrates a reinforced concrete specimen submerged in an electrolyte while both rebars are connected to a DC power supply with a constant current of 20 mA to accelerate the corrosion. For safety, the accelerated testing was stopped when the specimen was subjected to corrosion testing. The carbon steel rebars were used as the anodic electrodes and the stainless steel rebars as the cathodic electrodes. Tafel tests were performed prior to initiating and disconnecting from current flow. The LPR tests and resistivity readings were done two or three times per week. Figure 3.4 shows the Gamry potentiostat used for corrosion testing and the DC power supply arranged to connect to 16 prisms in series. The white cables are connected to the carbon steel, and the black cables are connected to stainless steel rebar.

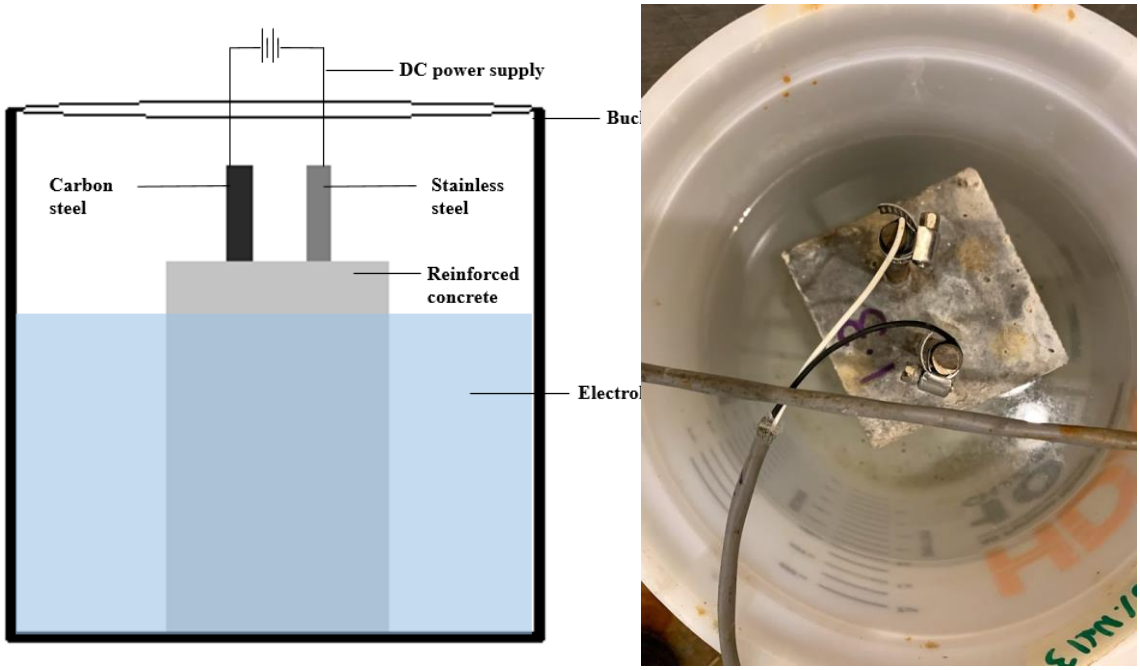

Figure 3.3 Accelerated Corrosion Testing Setup

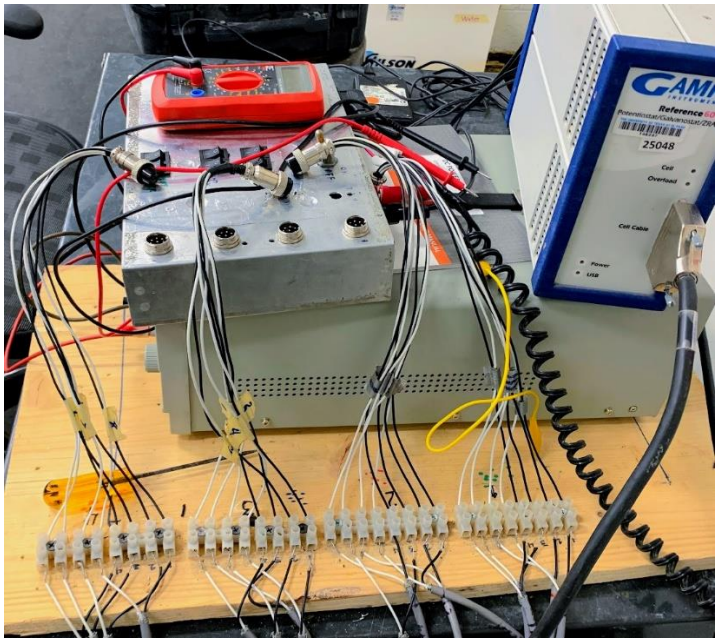

Figure 3.4 Gamry Potentiostat and DC Power Supply

Electric Resistivity

The electric resistivity indicates the probability of corrosion of the concrete. High electric resistivity is interpreted as low corrosion potential, and low electric resistivity results in high corrosion rate. The inverse of resistivity is conductivity. As shown in Figure 3.5, a four probe Wenner configuration was used to determine the electric resistivity of the concrete. A handheld device manufactured by Proseq with a spacing between probes of 50 mm was used. In the Wenner configuration, a current is emitted from the first probe to the fourth probe through the concrete, while the two inner probes measure the potential difference as shown in Figure 3.5. The instrumentation automatically calculates the resistivity from:

$$\rho = \frac{2\pi aV}{I} \tag{3.1}$$

where ρ = resistivity (Ω•m), a = Electrode separation (m), V = Voltage (V) and I = current (amp)

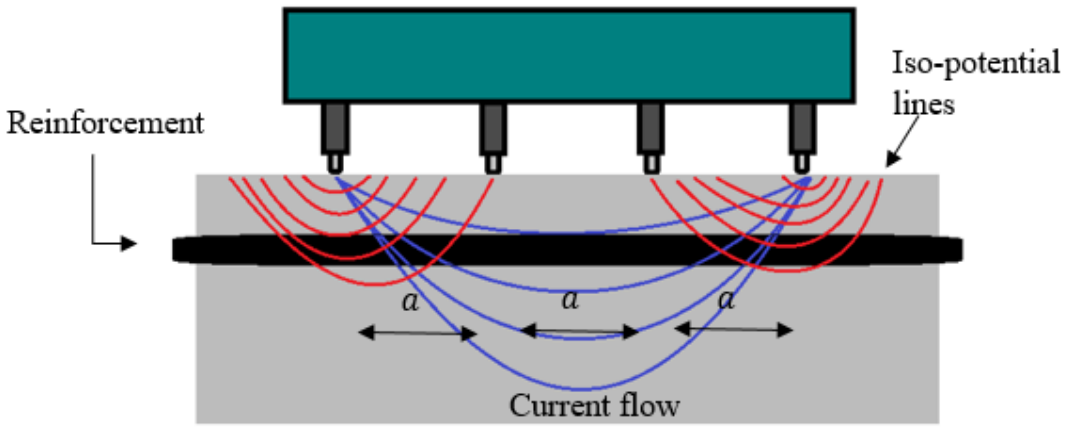

Figure 3.5 Electrical Resistivity Instrumentation for Reinforced Concrete

Table 3.3 shows approximate relationship between the resistivity and the corrosion activity of the rebar is used to interpret the results. The interpretation of results can be difficult since the

resistivity can be affected by chloride diffusion, temperature, moisture content, delamination, or porosity (Gucunski et al, 2013).

Table 3.3 Electrical Resistivity and Corrosion Activity (Gowers & Millard, 1999)

Electrical Resistivity (kΩ•cm)	Corrosion Rate
< 5	very high
> 5	high
5-10	moderate - low
>20	low

The Electrical Resistivity can be performed multiple times, which is ideal for testing the heterogeneous body of reinforced concrete. Resistivity readings were taken every day during the 14-day-curing-period, and every two to three days during the accelerated corroding period. Figure 3.7 demonstrates the top view of the reinforced cut into 4 prisms. The resistivity readings were carried out in the blue areas. The average of five resistivity readings for each prism were calculated per day. For accurate readings, a small amount deionized water was sprayed on the surface of the concrete before taking a reading.

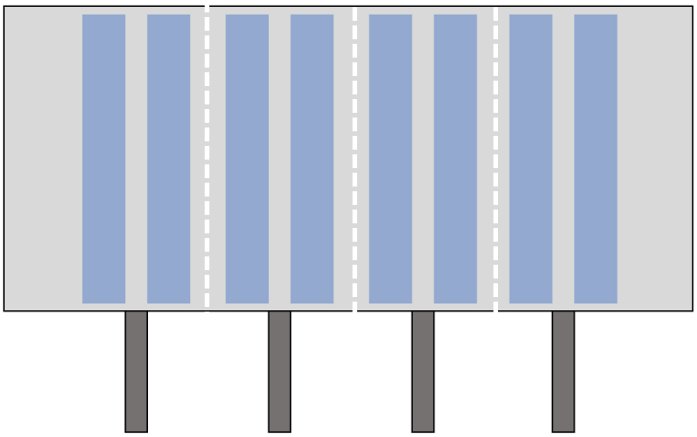

Figure 3.6 Resistivity Reading Areas

Electrochemical Corrosion Monitoring Techniques

The electrochemical techniques monitor corrosion via a potentiostat. A three-electrode configuration consisting of a working electrode (WE), a counter electrode (CE), and a reference electrode (RE), was used in this study. The working electrode was the carbon steel rebar, the counter electrode was the stainless-steel rebar, and the reference electrode was a Copper/Copper-Sulfate electrode. The electrodes were connected to the potentiostat with alligator clips (Figure 3.7). The Tafel and LPR electrochemical tests were used to measure corrosion of the working electrode. The sponge of the reference electrode was wetted with a 3.5% chloride solution sprayed on the concrete surface to ensure contact and flow of the copper-copper-sulfate reference electrode to the concrete.

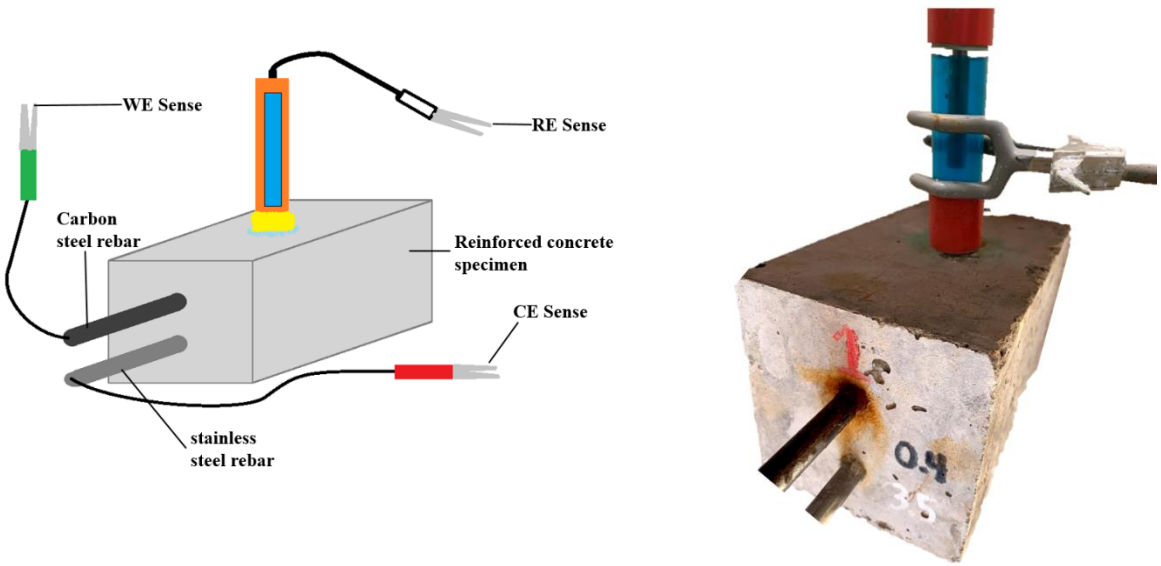

Figure 3.7 Linear Polarization Electrode Setup

In the LPR technique, the rebar is polarized with a range of 20 mV relative to the open circuit (OC) potential to generate a current flow between the working electrode and counter

electrode. The OC potential is the difference in electric potential between the working electrode and the reference electrode with no current flow.

Figure 3.8 shows a typical linear polarization resistance plot. The testing procedure took approximately 3 minutes to acquire the slope shown in Figure 3.8. The slope where the current is equal to zero is used to calculate the corrosion current using the Stern-Geary equation (Stern-Geary, 2016):

$$Rp = \frac{\Delta E}{\Delta i} = \frac{\beta a \beta c}{2.3\ icorr(\beta a + \beta c)} \tag{3.2}$$

where Rp = polarization resistance (Ω), ΔE = potential difference (V), Δi = current difference (A) βa = anodic slope, βc = cathodic slope and $icorr$ = corrosion current (A). The anodic and cathodic slopes (βa and βc) can be determined more accurately using the Tafel technique. If Tafel slopes are not calculated then the slopes will remain constant with a value of 0.12 $^{V}/_{Dec}$, leading to the equation below (Popov, 2015):

$$I_{corr} = \frac{0.026}{R_p} \tag{3.3}$$

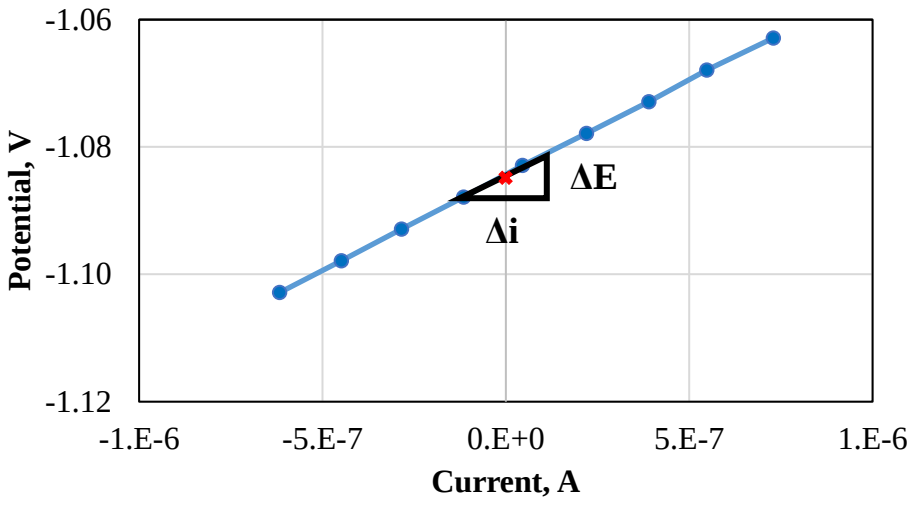

Figure 3.8 Linear Polarization Resistance and Characteristics

After calculating the current density, the last step is to calculate the corrosion rate using:

$$CR = \frac{I_{corr} KEW}{dA} \tag{3.4}$$

where CR = Corrosion rate, K = constant that defines the units for the corrosion rate, EW = Equivalent weight (g/equivalent), d = density (g/cm^3) and A = Area (cm^2). The constant value K is equivalent to 3.272×10^6 if the corrosion is calculated in microns.

Tafel Exploration

The Tafel test is the continuation of the LPR plot as shown in Figure 3.9. The Tafel plot shows the LPR region and the measurement of the Tafel constants (βa and βc) which are the slopes of each anodic and cathodic slope. The intersection of the anodic slope and cathodic slope gives the corrosion current density (A/cm^2) of the working electrode.

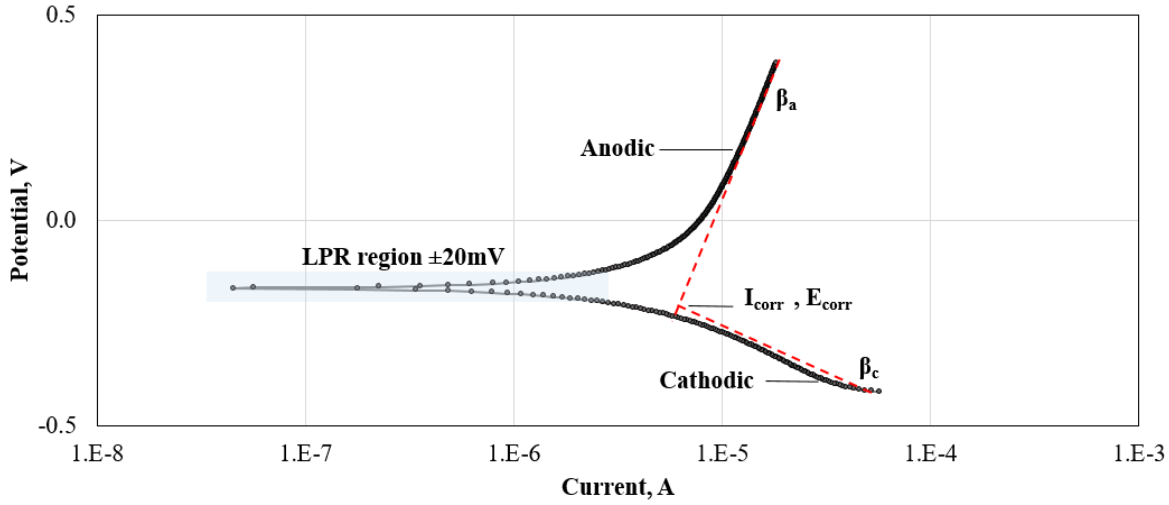

Figure 3.9 Tafel Plot

The Tafel method applies a potential shift of ±250 mV and can increase the corrosion of the rebar during the electrochemical technique; therefore, the Tafel is considered a semi-

destructive method. It is recommended to perform the Tafel test limited times. The Tafel tests that were carried out at a voltage scan rate of 1 mV/s took approximately 13 minutes.

The Tafel technique used analyzes the Tafel plot over a ±130 mV window of over-potentials to assimilate an LPR region. The Bulter-Volmer fit equation shown below is used to estimate the corrosion current density (Böhni, 2005):

$$I_{corr} = i_0 \left(e^{\frac{-\propto_{AnFN}}{RT}} - e^{\frac{-\propto_{cnFN}}{RT}} \right) \tag{3.5}$$

where $\propto_A$ = anodic charge transfer coefficient, $\propto_B$ = cathodic charge transfer coefficient, i_0= exchange current density (A/m^2), T= absolute temperature (K), R= universal gas constant, F = Faraday constant, N = activation over-potential, $n =$ number of electrons in the reaction, and $Icorr =$ corrosion current density (A/m^2). As for LPR, the last step is to calculate the corrosion rate from the corrosion current density using Equation 3.4.

Diameter Loss

The LPR and Tafel corrosion rates were used to estimate the average diameter loss of each carbon steel rebar, assuming a uniform corrosion depth along the rebars. The accumulation of corrosion on the rebar is demonstrated in Figure 3.8. . The rebar's radius is reduced from the initial radius R_i (nominally equal to 3/16 in. or 4673 μm) to R_f because of the corrosion of the iron in the carbon steel rebar. The outer diameter is the oxide layer that builds up around the rebar, R_r, was estimated by summing the corrosion rates obtained from the LPR or Tafel multiplied by the time between consecutive measurement. The diameter loss was then calculated from:

$$Diameter\ Loss(\%) = \left(\frac{\mathrm{Rr}}{R_i}\right) \times 100 \tag{3.6}$$

As a check on the reasonableness of the estimated corrosion losses with the two methods, the final weight of the rebar after removing the rust layer along the unit weight of carbon steel were used to estimate R_r.

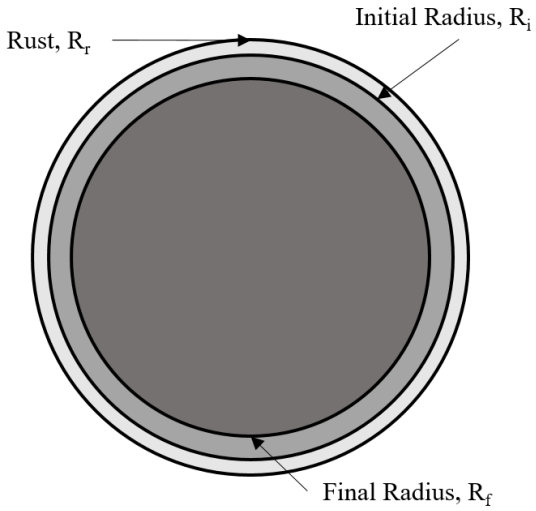

Figure 3.10 Diameter Loss of Carbon Steel Rebar Due to Corrosion

Chapter 4. Results and Discussions

The Tafel test, LPR and electrical resistivity measurements were carried out and compared to the actual corrosion of embedded rebars to establish a correlation among the results of the electrochemical measurements of the reinforced concrete under altered environment conditions and concrete mixes. These correlations will help in understanding the limitations and strengths of those methods in estimating the service lives of the reinforced concrete structure for repair or maintenance due to corrosion. The example results shown in this chapter is for two concrete specimens. One concrete specimen was submerged in tap water and the other was submerged in 3.5% sodium chloride solution.

4.1 Electrical Resistivity

The examples of electrical resistance readings taken during the 14-day curing period in the moisture conditioning room and 28-day-testing period for Batch 9 and 10 (Table 3.1) are shown in Figure 4.1. Batch 9 was submerged in tap water with an average conductivity of 200 μSiemens, and Batch 10 was submerged in 3.5% sodium chloride solution with a very high (out of range) conductivity. Each point represents the average of 20 resistivity readings as discussed in Chapter 3. The error bars correspond to ±1 standard deviations of the measured values. The results are similar with small variations within and among the specimens for the first 14 curing days. The resistivity of the specimens increases with time during curing. After day 7 of testing period (day 21 in Figure 4.1), the resistivity readings for prisms submerged in sodium chloride solution began to decrease gradually due to chloride ions penetrating into the concrete, and the resistivity of the prisms submerged in tap water began to increase rapidly since concrete made with Portland cement will harden even if it is completely under water (Lau, 2001).

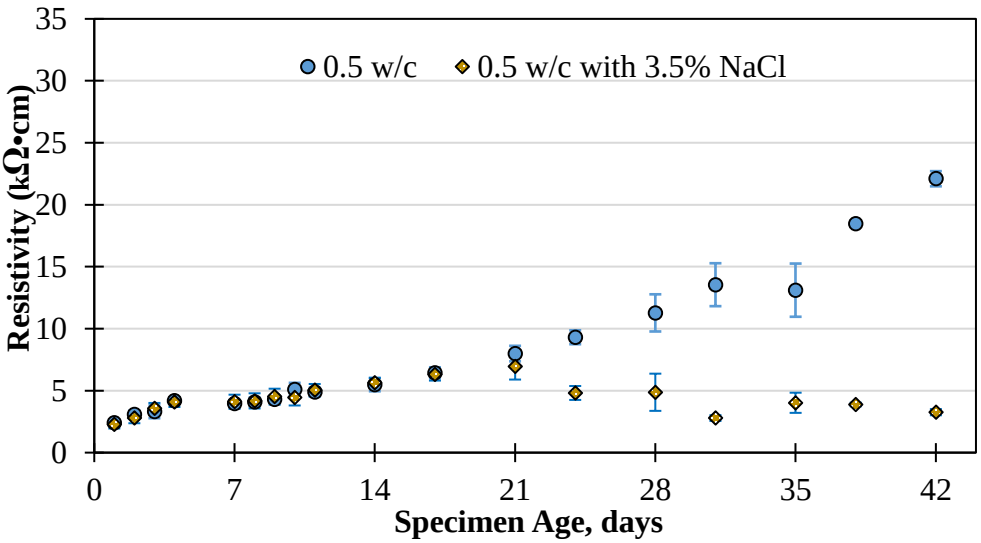

Figure 4.1 Typical Resistivity Results

Figure 4.2 demonstrates the average resistivity of each of the four prisms cut from the two specimens after the 14-day cuing-period. For both specimens, the four prisms initially demonstrate similar patterns. For the specimens submerged in tap water, the resistivity values gradually increase as shown in Figure 4.2a. As signified with the dotted bars in the figure, the pattern in increase in the resistivity changes as soon as the specimens are disconnected from the amperage and not placed in the water any further. The resistivity values of the prisms submerged in the high chloride content fluid changes around day 7, as shown in Figure 4.2b. Again, the prisms connected to the voltage while submerged in the high chloride fluid signified with solid bars, exhibited a decrease in the resistivity with time. However, as soon as a given prism is disconnected from amperage and not submerged any more (dotted bars), the resistivity increased with time. The lowest resistivity was observed for the Prism 4 submerged in the chloride solution and the highest resistivity for the Prism 1 that was only submerged in water for 7 days and then allowed to dry for additional 21 days.

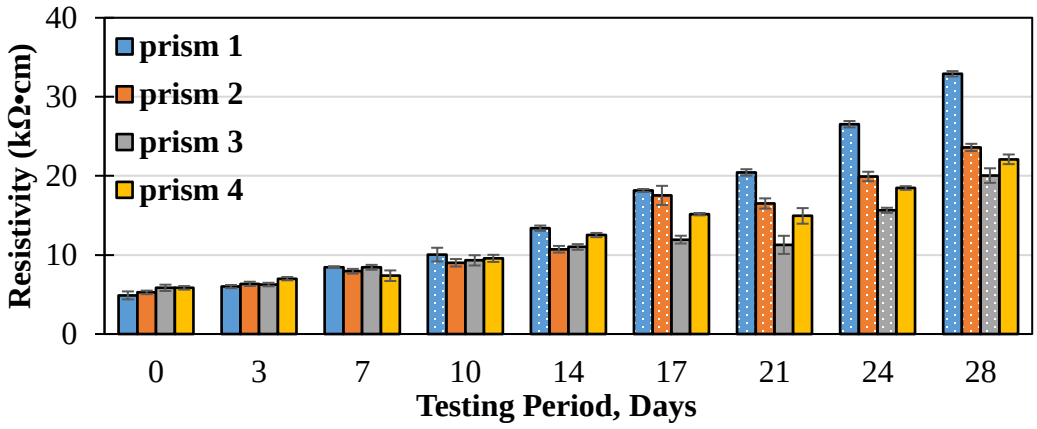

(a) Concrete Prisms Submerged in Tap Water

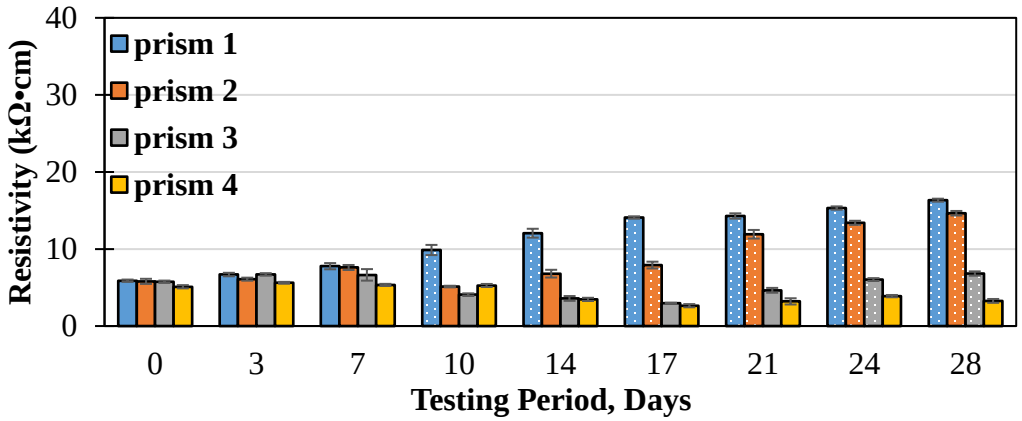

(b) Concrete Prisms in 3.5 % Sodium Chloride Solution

Figure 4.2 Resistivity Readings during Testing-Period

4.2 Voltage Measurements

The voltage readings taken during the 28-day-testing period for Batch 9 and 10 are shown in Figure 4.3. The number of voltage readings for the prisms embedded in either the tap water or chloride solutions are similar for each sets of measurements. As time passes by and as the number of prisms attached to voltage decreases, the voltage readings increase with time for the specimens submerged in tap water and decreases for those submerged in chloride solutions, to maintain a constant current of 20 mA. These patterns makes sense if one considers the fact that all the electrodes are setup in

a series loop with a constant current of 20 mA and that resistivity and voltage are linearly proportional.

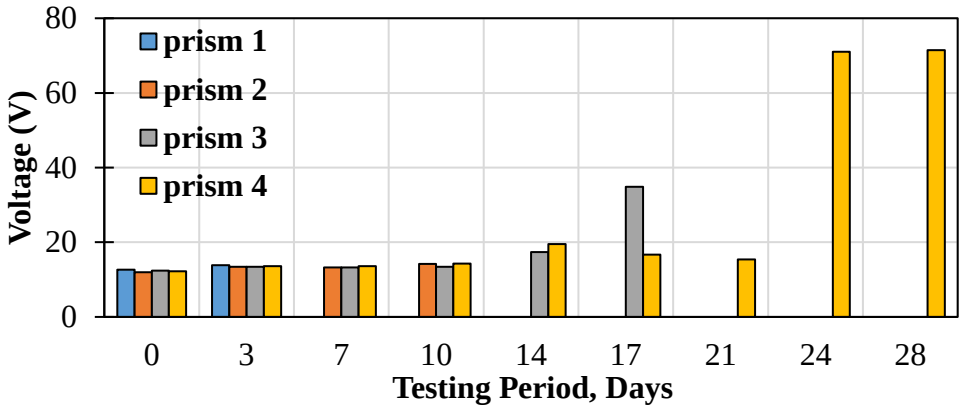

(a) Concrete Prisms Submerged in Tap Water

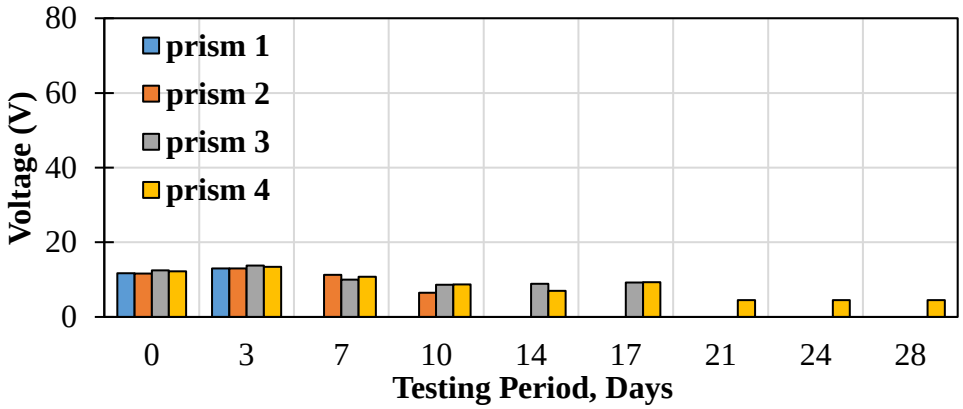

(b) Concrete Prisms Submerged in 3.5 % Sodium Chloride

Figure 4.3 Voltage Readings during Testing-Period

4.3 Linear Polarization Resistance (LPR)

The corrosion rates obtained from LPR with time are shown in Figure 4.4 for the two sets of specimens. Each bar represents the average of two LPR readings. The prisms submerged in the chloride solution exhibited substantially higher corrosion rates that increased further with time.

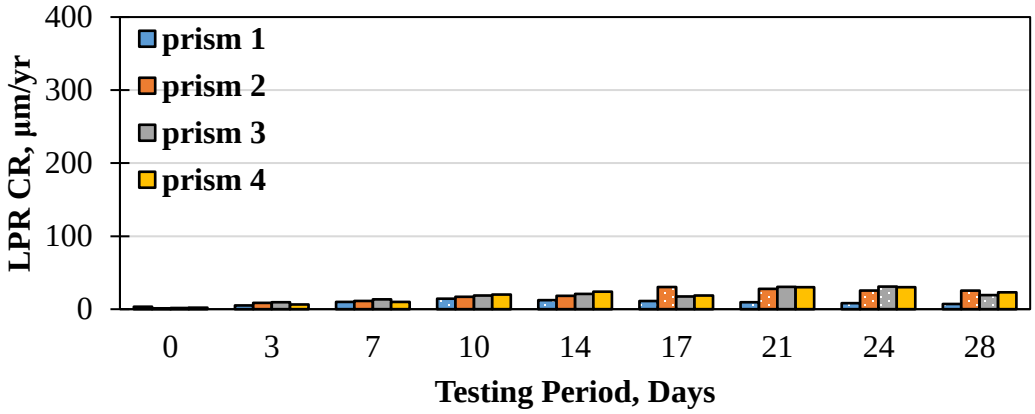

(a) Concrete Prisms Submerged in Tap Water

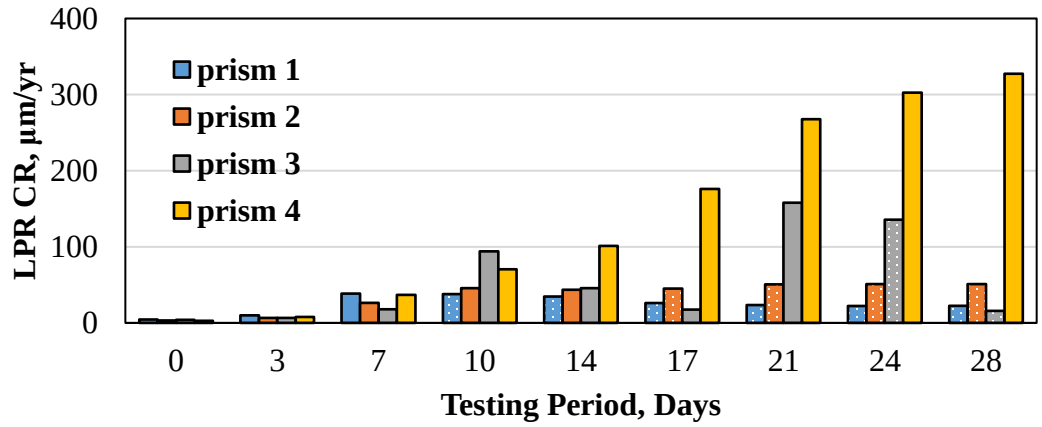

(b) Concrete Prisms Submerged in 3.5% Sodium Chloride

Figure 4.4 Linear Polarization Corrosion Rate Readings during Testing-Period

The measurements on the prisms that were disconnected and removed from the corresponding solutions, signified with dotted bars, began to decrease and later became constant. Prism 4 for both batches had the highest corrosion rate readings. As resistivity and voltage decreased, the corrosion rates increased.

4.4 Tafel

The corrosion rates obtained by the Tafel tests with time are shown in Figure 4.5. Given the semi-destructive nature of Tafel tests, they were carried out less frequently than the LPR tests. Three Tafel readings were performed one each prism, one on Day 0, one on the day it was disconnected from voltage (e.g., Prism 1 on Day 7), and another on Day 28. Tafel corrosion rates were comparable to LPR corrosion rates. The prisms submerged in the chloride solution exhibited higher corrosion rates that increased with time. Prism 4 submerged in chloride solution demonstrated the highest corrosion rate of 400 μm/yr at Day 28. Week 1 prism submerged in the tap water demonstrated the lowest corrosion rate. When all prisms were disconnected at day 28, the corrosion rate decreased except for the Prism 4 as seen in Figure 4.5.

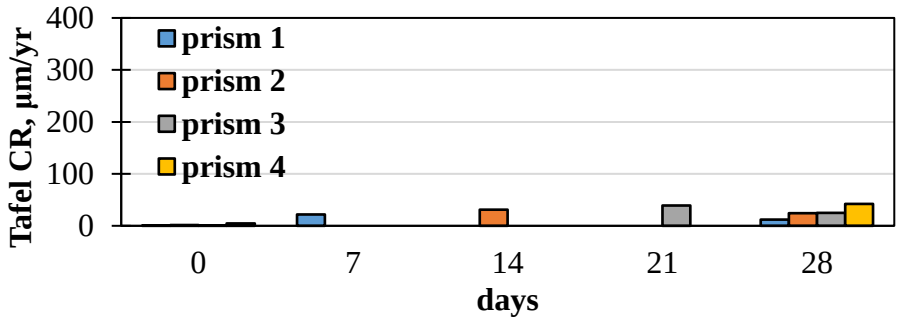

(a) Concrete Prisms Submerged in Tap Water

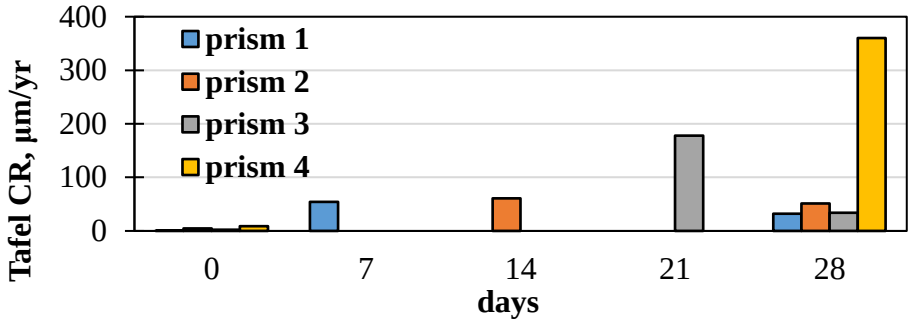

(b) Concrete Prisms Submerged in 3.5 % Sodium Chloride

Figure 4.5 Tafel Corrosion Rate Readings during Testing-Period

4.5 Change in Diameter of Reinforcement

The average diameter loss of the carbon steel rebar extracted from each prism obtained from LPR corrosion rates, Tafel corrosion rates and from weight-loss are compared in Figure 4.6. The estimated accumulated corrosion from the LPR and Tafel readings were very low (about 3% of those submerged in tap water and 5% of those submerged in sodium chloride solution) compared to the actual diameter loss. The diameter losses of the rebars submerged in 3.5% sodium chloride solution were greater than the diameter losses for rebars submerged in tap water.

The reason for the disparity between the electrochemical and weight loss method can be explained through Figure 4.7 as discussed by (Hœlér et al., 2004). The rust layer is composed of iron oxy-hydroxides and other oxides such as lepidocrocite (γ-FeOOH), goethite (α-FeOOH) and magnetite (Fe_30_4). Lepidocrocite is a semiconductor with electrochemically active species, goethite is an insulator, and magnetite is a good conductor but considered as protective due to its denser characteristics than either lepidocrocite or goethite (Hœlér et al., 2004). Although the development of the rust layer is not the focus of the present study, the electrochemically deposited layer is probably more compact and thinner than the actual corroded layer acquired without surface activation.

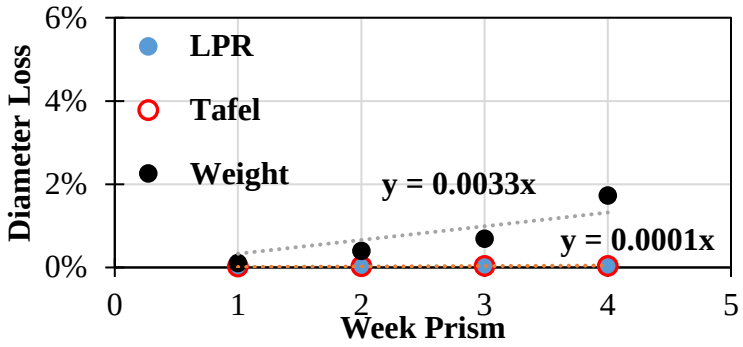

(a) Concrete Prisms Submerged in Tap Water

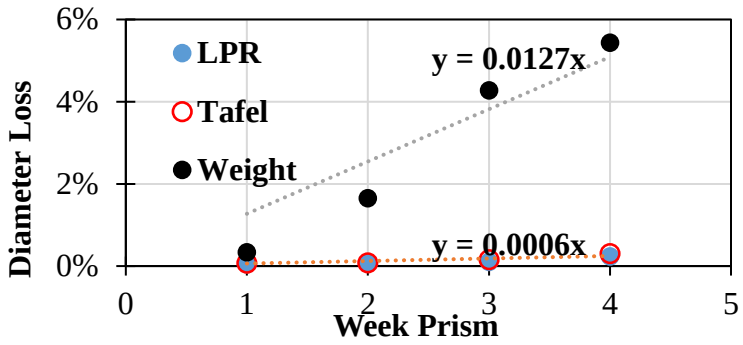

(b) Concrete Prisms Submerged in 3.5 % Sodium Chloride

Figure 4.6 Comparison of Diameter Loss Techniques

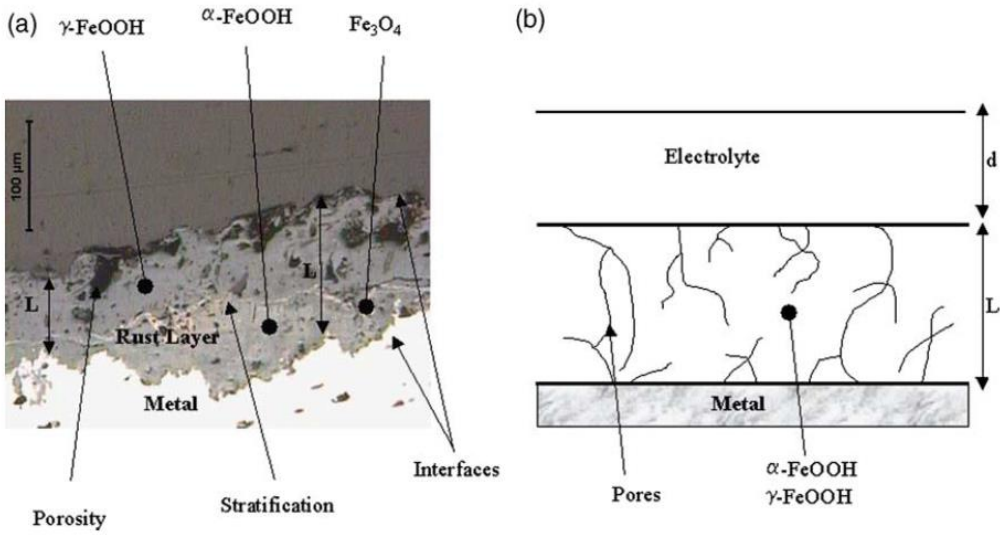

(a) Micrograph **(b) Sketch of Micrograph**

Figure 4.7 Rust Layer Characteristics Observed under SEM (Hœlér et al., 2004)

4.6 Visual Observations and Results

Figure 4.8 demonstrates four concrete prisms submerged in 3.5% NaCl solution for one to four weeks. All four specimens exhibited longitudinal cracks on top in the proximity of the carbon steel. The lengths of the cracks varied from around 4 in. to 7 in. after 1 and 2 weeks, respectively. The lengths of the cracks for the two specimens submerged for 3 and 4 weeks extended over the lengths of the specimens. The cracks became wider as the duration of submergence increased. The rust stains also become more prominent as the length of submergence increases

(a) Week 1 (b) Week 2 (c) Week 3 (d) Week 4

Figure 4.8 Conditions of the Reinforced Concrete Prisms with Duration of Submergence

Figure 4.9 demonstrates the four carbon steel reinforcements embedded in the four prisms shown in Figure 4.8. The rebars progressively corroded more with increasing the duration of submergence. Figure 4.8 coincides with the diameter loss shown in Figure 4.6b.

Figure 4.9 Progression of Corrosion of Carbon Steel Rebars with Duration of Submergence

4.7 Parametric Study

The LPR technique was used to monitor the corrosion of carbon steel rebars and the electrical resistivity method was used to measure the extent of the reinforcement affected by relative humidity, chloride concentration, water-cement ratio, aggregate type and cement type. The trends observed from this activity are described this section.

Influence of Humidity

Three similar specimens were subjected to three humidity regimes. One specimen was submerged in tap water, one was placed in an environmental chamber set to a relative humidity of 40%, and the third specimen was placed in a chamber with a relative humidity of 90%.

The average resistivity values of the specimens submerged in the tap water were compared with those of the specimens exposed to a 40% and 90% relative humidity, as shown in Figure 4.10.a. Specimens subjected to a relative humidity of 40% exhibit about 1.7 times greater resistivity values as compared to those submerged in tap water. On the other hand, the specimens subjected to relative humidity of 90%, exhibited resistivity values that are similar or less than those from the specimens submerged in tap water.

Figure 4.10b demonstrates the average corrosion rates obtained from the LPR measurements of the specimens subjected to the three humidity regimes. The rebars submerged in the tap water exhibited a higher corrosion rate as compared to rebars exposed to 40% or 90% relative humidity. The corrosion rate for the rebars exposed to a relative humidity of 40% are about 36% of those submerged in tap water. The rate of corrosion of those rebars on average are about 69% of the rebars submerged in the tap water. The humidity influences the corrosion but less than that acquired for specimens submerged in tap water.

Figure 4.10c compares the average diameter loss for the specimens submerged in tap water obtained from the weight loss technique with those from specimens subjected to 40% and 90% relative humidity. Rebars submerged in the tap water exhibited significantly higher diameter loss as compared to those exposed to 40% or 90% relative humidity. The diameter loss for the rebars exposed to a relative humidity of 40% are about 8% of those submerged in tap water. The diameter loss for rebars exposed to a relative humidity of 90% are about 40% of those submerged in water.

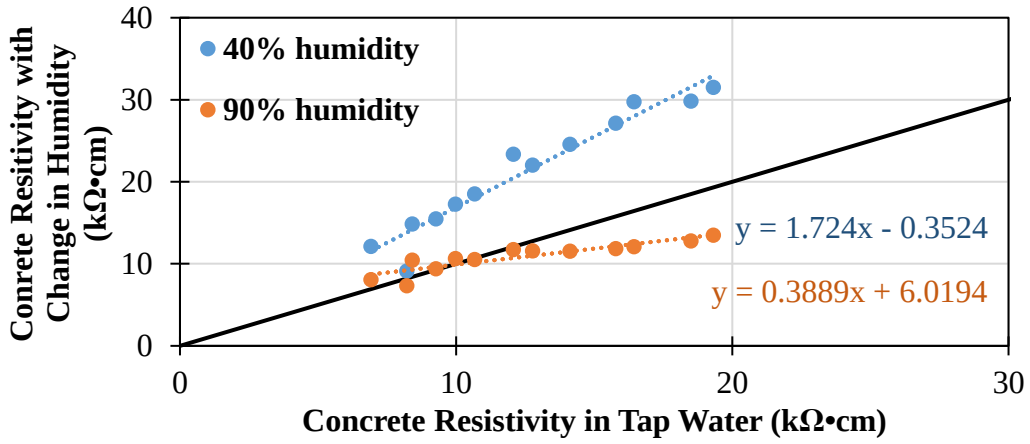

(a) Electrical Resistivity

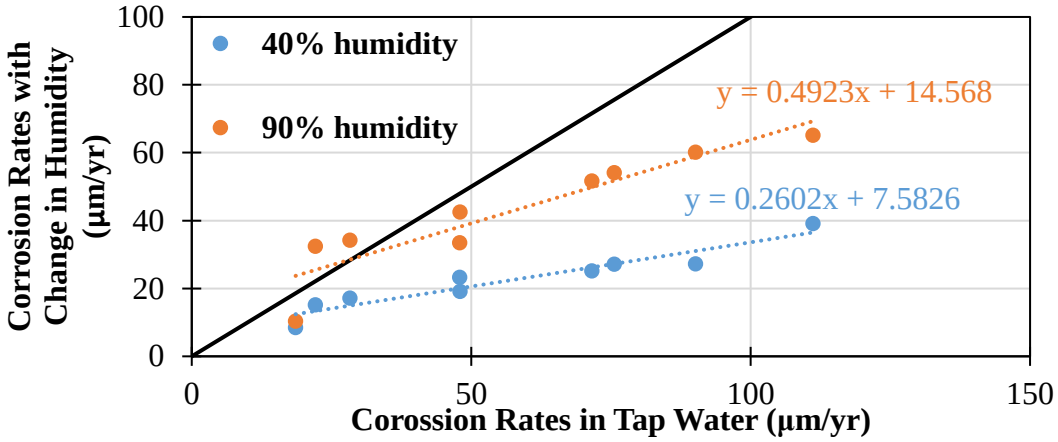

(b) Corrosion Rates Obtained from LPR

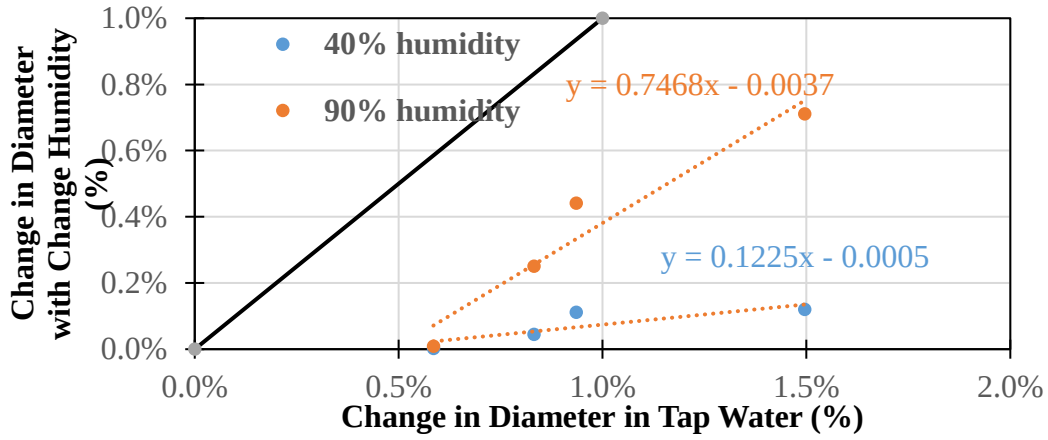

(c) Diameter Loss

Figure 4.10 Influence of Humidity on Properties of Concrete and Rebars

Influence of Chloride Concentrations

To study the impact of chloride concentration, three specimens were submerged in tap water, in 3.5 % sodium chloride solution and in 10.5 % sodium chloride solution. As shown in Figure 4.11a, the average resistivity values of the specimens submerged in 3.5% and 10.5% sodium chloride solutions exhibited divergent patterns relative to the resistivity values of the specimens submerged in tap water. As the resistivity values of the specimens in tap water increase significantly, the resistivity values of the other two specimens decrease slightly.

Figure 4.11b demonstrates the average corrosion rates obtained from the LPR measurements of the specimens submerged in the three liquids with the three chloride concentrations. The rebars submerged in the tap water exhibited the lowest corrosion rates as compared to the rebars submerged in the liquids with the two higher chloride concentrations. The rebars submerged in 3.5% and 10.5% sodium chloride solutions experience corrosion rates that are exponential as compared to those submerged in tap water.

Figure 4.11c demonstrates the average diameter loss, obtained from the weight loss technique for the specimens submerged in tap water, 3.5% and 10.5% NaCl solutions. Rebars submerged in tap water exhibited the lowest diameter loss as compared to those submerged in 3.5% and 10.5% sodium chloride solutions. The rebars submerged in 3.5% and 10.5% sodium chloride solutions experience around the same change in diameter. Since the saturation degree of NaCl in water is about 1.2%, any higher chloride constructions might not influence the rates of corrosion. The diameter loss for the rebars submerged in 3.5% and 10% NaCl solutions are about eight to nine times of those submerged in the tap water.

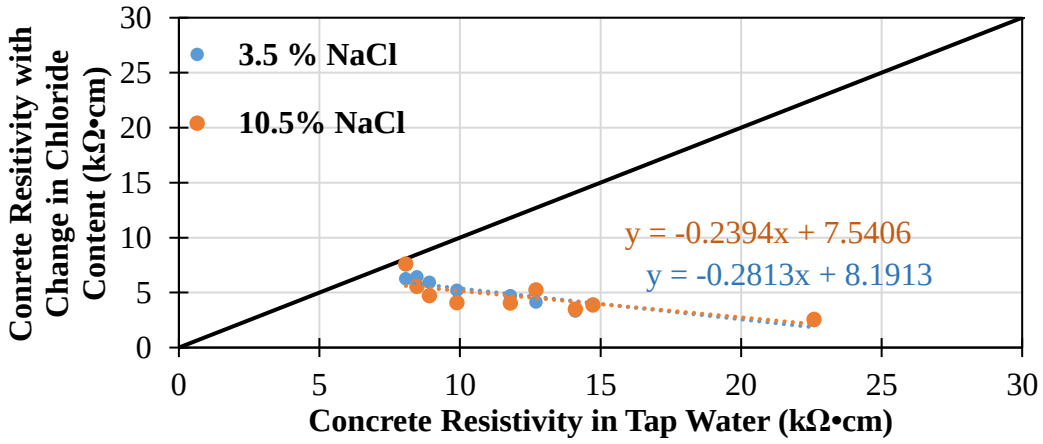

(a) Electrical Resistivity

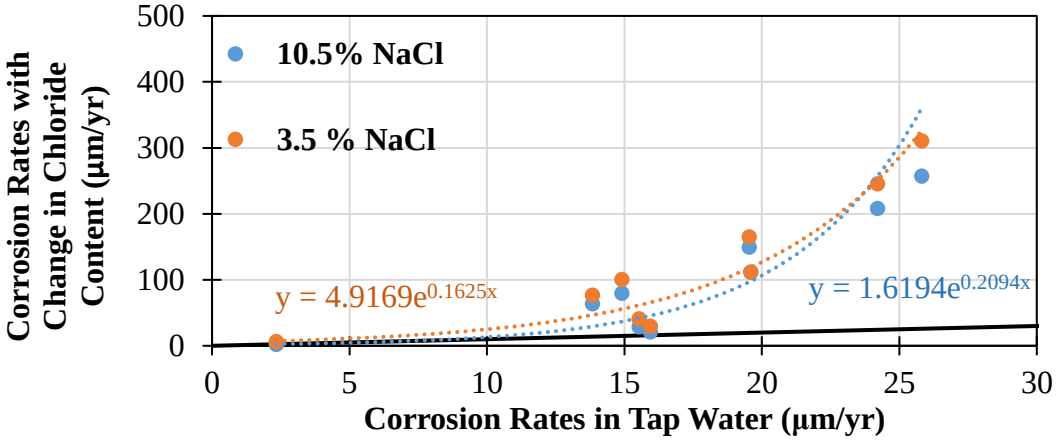

(b) Corrosion Rates Obtained from LPR

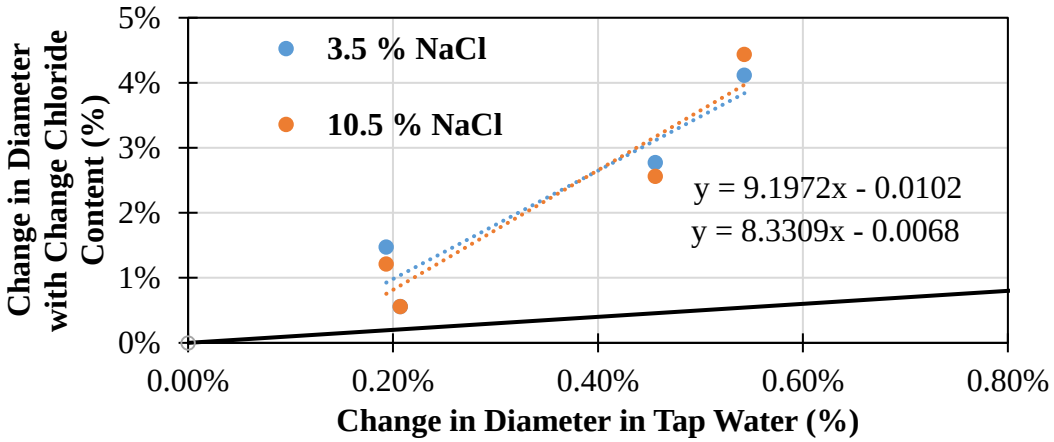

(c) Diameter Loss

Figure 4.11 Influence of Chloride Concentration on Corrosion of Rebars

Influence of Chloride Concentrations within Concrete Mix

Four specimens were prepared with solutions containing 0.8%, 1.6% and 2.4% sodium chloride, during mixing to represent the preparation of concrete with saltwater. These specimens and one specimen without chloride in the concrete were submerged in tap water during curing and testing. The average resistivity values of the concrete specimens could not be measured.

Figure 4.12a demonstrates the relationships among the average corrosion rates obtained from the LPR measurements of the specimens spiked with NaCl with those prepared with no additional NaCl. The corrosion rates for the rebars embedded in concrete with 0.8%, 1.6% and 2.4% salt are about 1.7, 1.8, and 2 times of those submerged in water.

Figure 4.12b demonstrates the average diameter loss obtained from the weight loss technique for the specimens submerged in tap water with 0.8%, 1.6%, and 2.4% NaCl within the concrete mix. Rebars within the normal concrete exhibited the lowest diameter loss as compared to those spiked with sodium chloride. The diameter loss for the rebars embedded in concrete mixed with 0.8%, 1.6% and 2.4% salt are about 5.6, 11.8 and 20 times of those with normal concrete.

Influence of Water Cement Ratio

Three specimens with water-cement (w/c) ratios of 0.4, 0.45, and 0.5 were submerged in tap water. The average resistivity values of the specimens with 0.45 w/c are compared in Figure 4.13a to the average resistivity values of the specimens with the 0.4 and 0.5 w/c. The average resistivity values for the specimens with the 0.4 w/c were the highest and are about 1.2 times greater than those of 0.45 w/c. Specimens with 0.5 w/c exhibited the lowest resistivity values that are about 93% of those from the specimens with 0.45 w/c.

Figure 4.13b demonstrates that the average corrosion rates obtained from the LPR measurements for rebars embedded in concrete with 0.4 w/c exhibited the lowest corrosion rate about 72% of those embedded in concrete with 0.45 w/c. The corrosion rates for the rebars embedded in concrete with 0.4 and 0.45 w/c are similar.

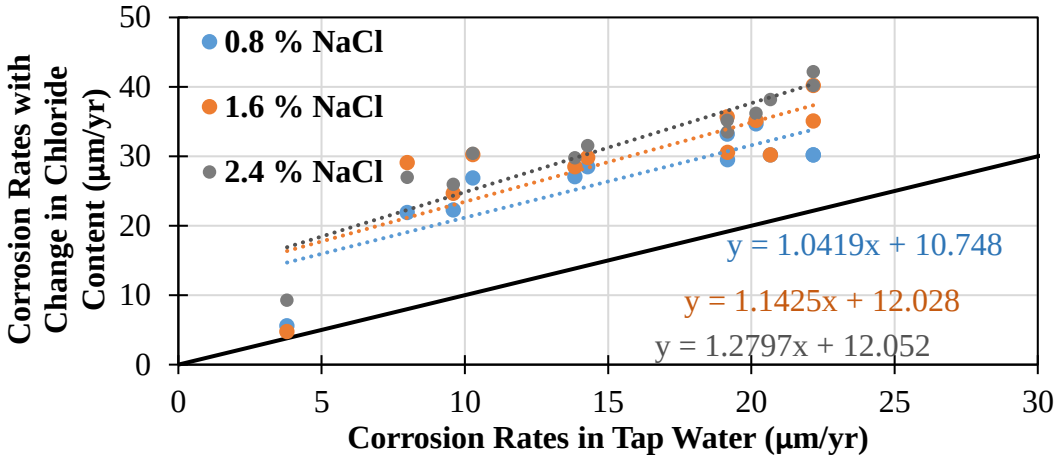

(a) Corrosion Rates obtained from LPR

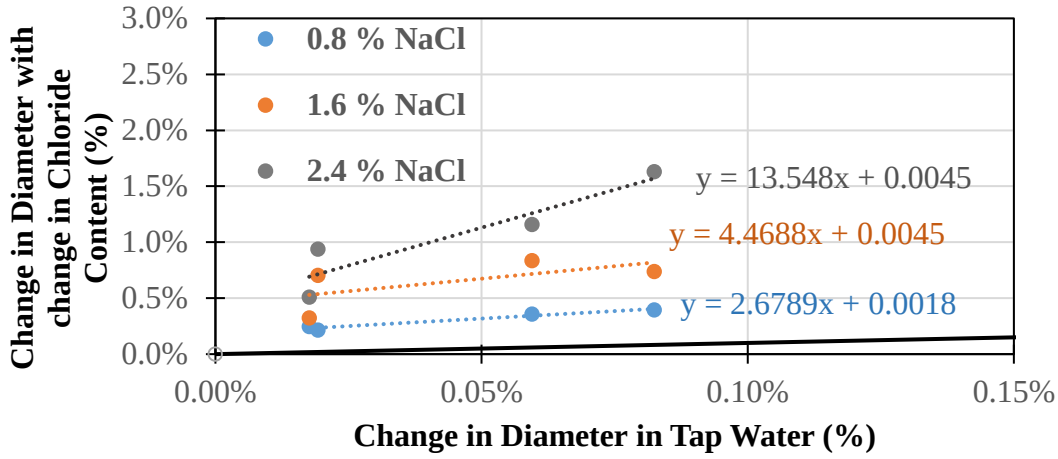

(b) Diameter Loss

Figure 4.12 Influence of Chloride Concentration on Properties of Concrete and Rebars

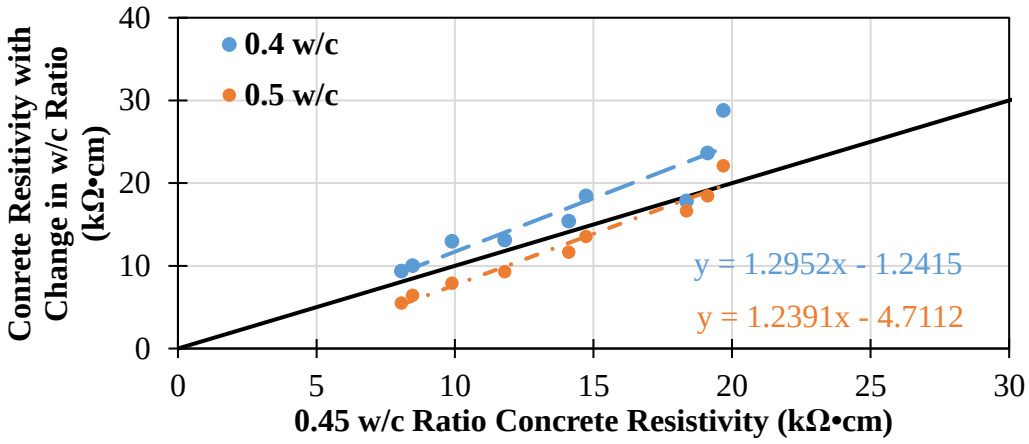

(a) Electrical Resistivity

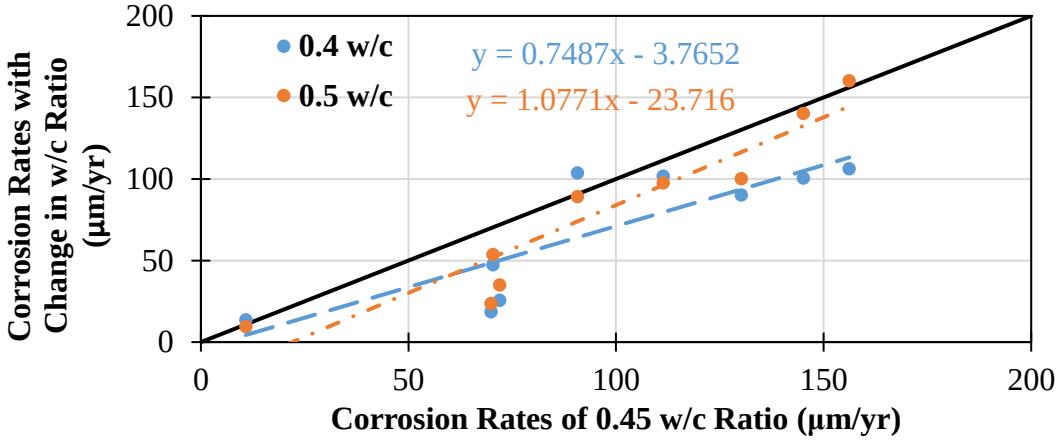

(b) Corrosion Rates Obtained from LPR

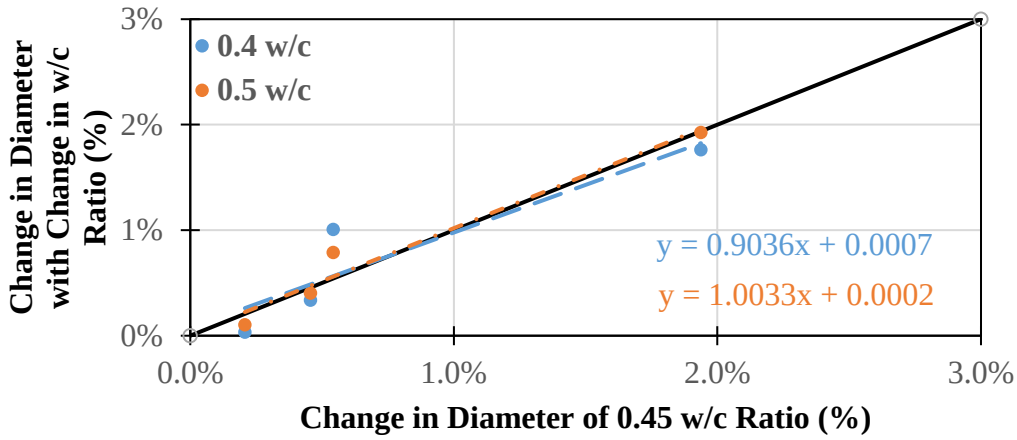

(c) Diameter Loss

Figure 4.13 Influence of Water-Cement Ratio (w/c) on Properties of Concrete and Rebars

Figure 4.13c compares the average diameter loss obtained from the weight loss technique for the specimens with 0.45 w/c to those specimens with 0.4 and 0.5 w/c. All rebars exhibited similar diameter loss. The diameter loss of the rebars embedded in concrete with 0.4 w/c were about 96% of those rebars embedded in concrete with 0.45 w/c. The diameter loss for the rebars embedded in concrete with 0.5 w/c are about 1.02 times of those rebars embedded in 0.45 w/c ratio. Agreeing to the results obtained from corrosion rates and electrical resistivity on Figure 4.13, a w/c ratio of 0.4 is ideal for embedding reinforcement to decelerate corrosion; higher w/c ratio will increase the corrosion rate of the rebars.

Influence of Aggregate Source

Two specimens with different aggregates, dolomite limestone and gravel, were submerged in tap water for testing. The average resistivity values of the specimens composed of gravel are compared in Figure 4.14a to the average resistivity values of the specimens composed with dolomite limestone. Specimens with gravel experience a higher resistivity values about 1.25 times than those with dolomite limestone.

Figure 4.14b demonstrates the average corrosion rates obtained from the LPR measurements of the specimens with dolomite limestone versus gravel. The rebars embedded in the concrete composed of gravel exhibited lower corrosion rate about 40% to rebars embedded in the concrete composed of dolomite limestone.

Figure 4.14c compares the average diameter loss obtained from the weight loss technique for the specimens with dolomite limestone to those specimens with gravel. The rebars embedded in concrete with gravel exhibited lower diameter loss, about 45% of those rebars embedded in dolomite limestone. Fine aggregate on concrete is more significant than coarse aggregate in the term of corrosion (Xiao, 2016).

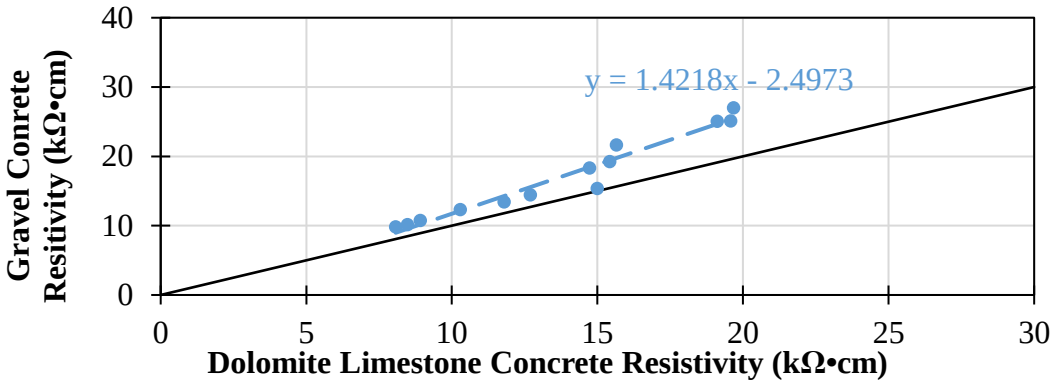

(a) Electrical Resistivity

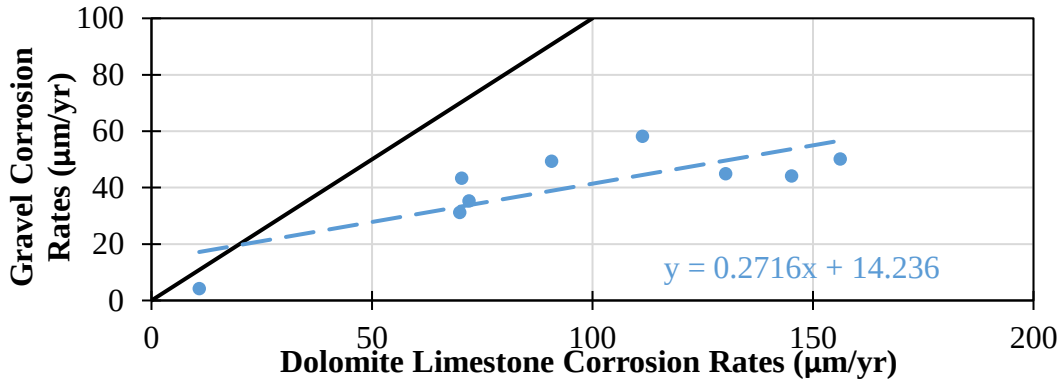

(b) Corrosion Rates Obtained from LPR

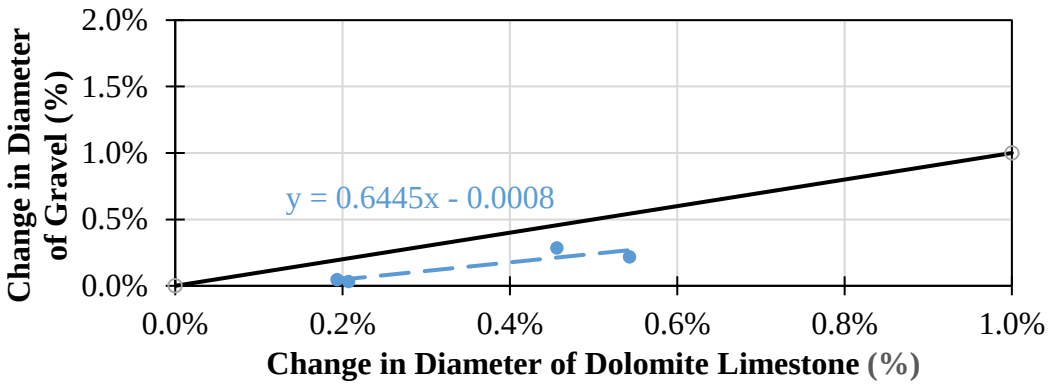

(c) Diameter Loss

Figure 4.14 Influence of Aggregate on Properties of Concrete and Rebars

Influence of Cement Type

The impact of change in cement from Type I/II to Type V is reflected in Figure 4.15. The concrete specimens that were made with dolomite limestone were submerged in tap water for testing. From Figure 4.15a, the average resistivity values of the specimens with Type V cement are slightly higher around 1.15 times than those with Type I/II cement.

Figure 4.15b demonstrates the average corrosion rates obtained from the LPR measurements of the specimens. The rebars embedded in concrete with Type V cement exhibited lower corrosion rates about 70% of the rebars embedded in concrete with Type I/II cement.

Figure 4.15c compares the average diameter loss obtained from the weight loss technique. The rebars embedded in concrete with Type V cement exhibit about 40% diameter loss than those rebars embedded in concrete with Type I/II cement. Concrete with Type V cement should impede the corrosion rate of the rebars due to the decrease of alkalinity in the cement, and increase the resistivity of the concrete.

4.8 Relation between Concrete Resistivity and Corrosion of Reinforcements

Figure 4.16 shows the relationships between the concrete's resistivity to the corrosion rate of the reinforcement for each experiment conducted in this study. A unique relationship cannot be observed indicating that several other environmental and materials parameters may impact the relationship between the resistivity of concrete and the corrosion of rebars. As demonstrated in Figure 4.16a, the corrosion rate is directly proportional to the resistivity for the specimens submerged in tap water. According to Hornbostel 2013, the resistivity increases with time since the concrete continues to harden under water, and the corrosion rate gradually increases in time since the rebars were connected to a power supply with a constant current that will degrade the reinforcement.

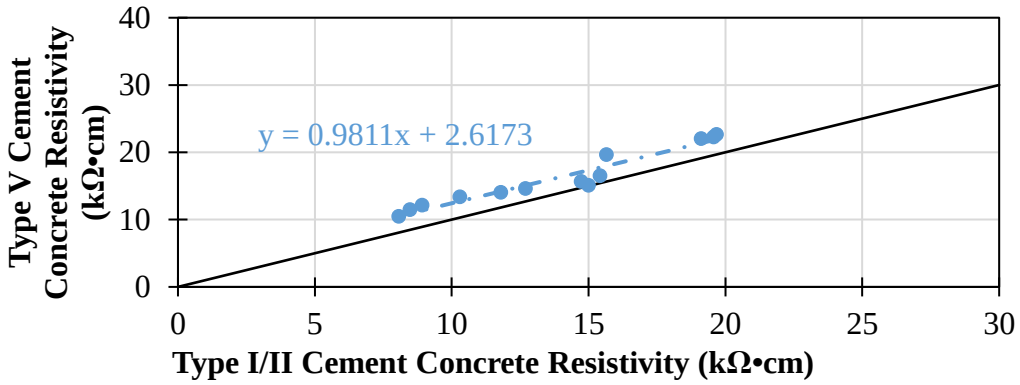

(a) Electrical Resistivity

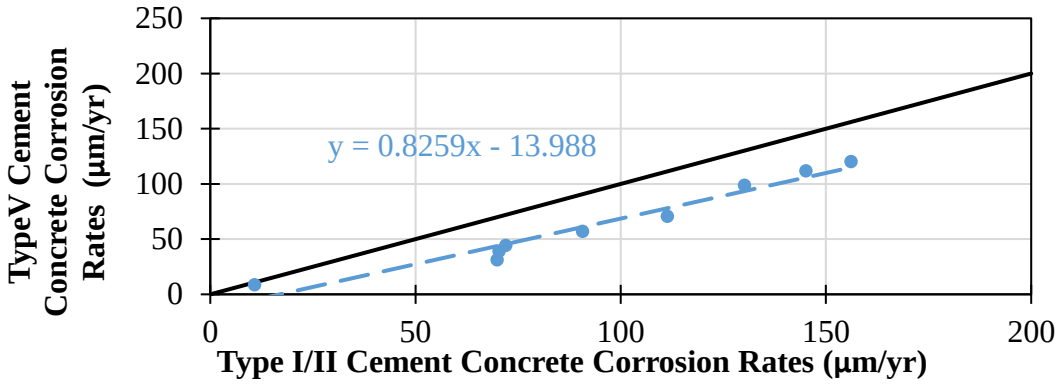

(b) Corrosion Rates Obtained from LPR

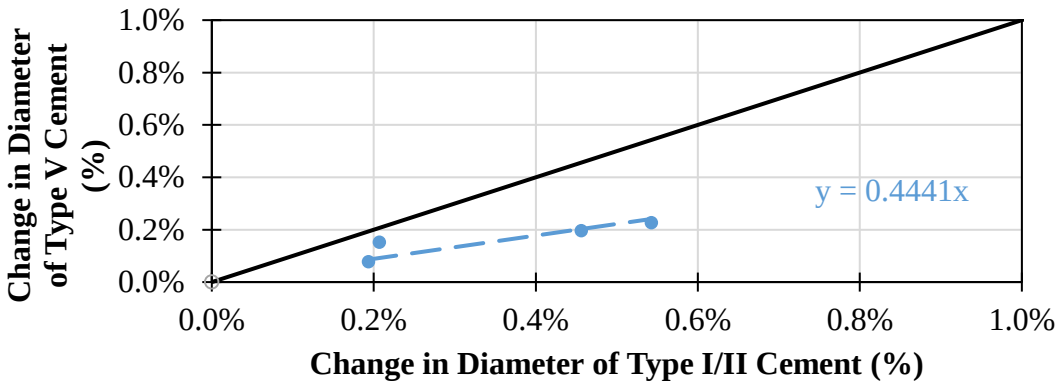

(c) Diameter Loss

Figure 4.15 Influence of Cement Type on Properties of Concrete and Rebar

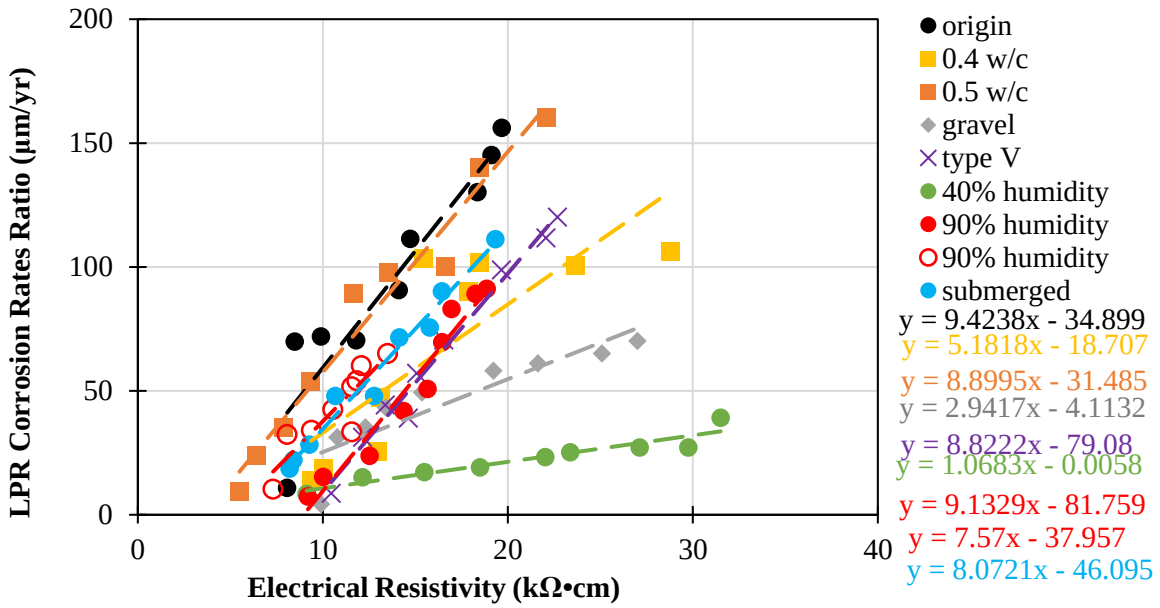

(a) Concrete Prisms submerged in Tap Water or Set inside Humidity Chamber

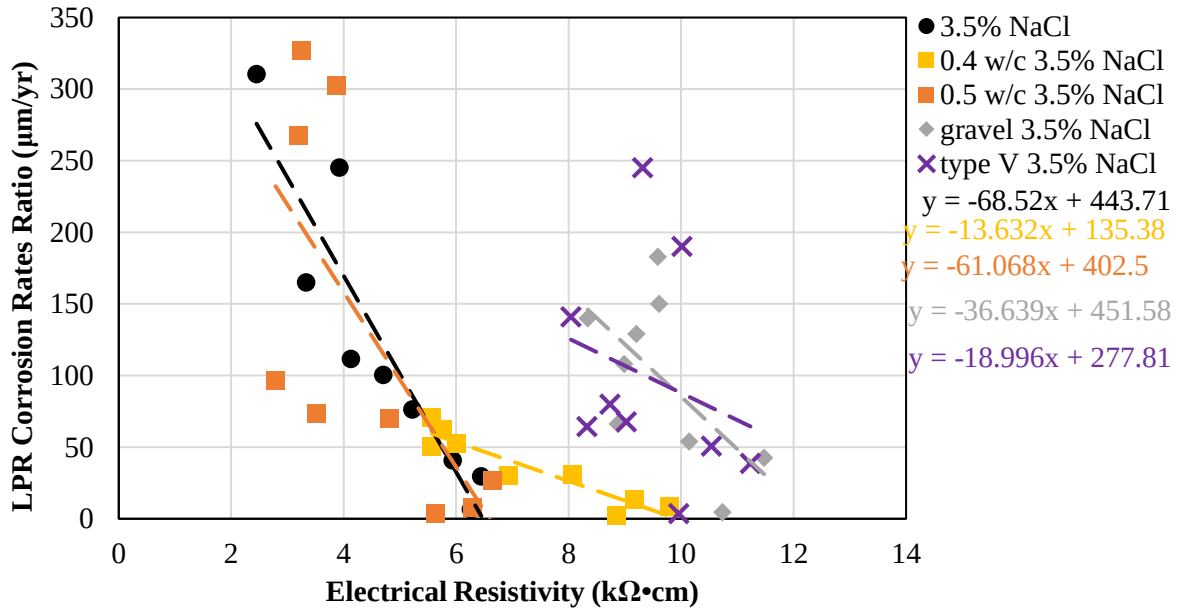

(b) Concrete Prisms Submerged in 3.5% NaCl Solution

Figure 4.16 Correlation of Concrete's Resistivity to the Reinforcement's Corrosion Rate

As shown in Figure 4.16b, a trend more representative of the classical observations of a low resistivity is related to a high risk of corrosion is observed when the specimens are submerged in NaCl solution (as opposed to tap water). Concrete specimens exposed to low humidity and composed of gravel showed less steep slopes when compared to the other conditions.

Figure 4.17 relates the concrete's resistivity to the diameter loss calculated by the weight loss of the reinforcement, under different conditions studied. Since the loss of diameter is proportional to Figure 4.16a, the concrete's resistivity and the degradation of the reinforcement increase with time. The diameter loss is directly proportional to the resistivity. The resistivity increases with time since the concrete continues to harden under water, and the diameter loss gradually increase in time since the rebars were connected to a power supply with a constant current that will degrade the reinforcement. On the other hand, prisms submerged in chloride show an inverse relationship for the concrete's resistivity and diameter loss. The results of Figure 4.17b are proportional to Figure 4.16b. The concrete's resistivity decreases and the degradation of the reinforcement increase with time. Concrete with 0.5 w/c ratio demonstrated the most degradation of the diameter for both figures, submerged in tap water and submerged in chloride solution.

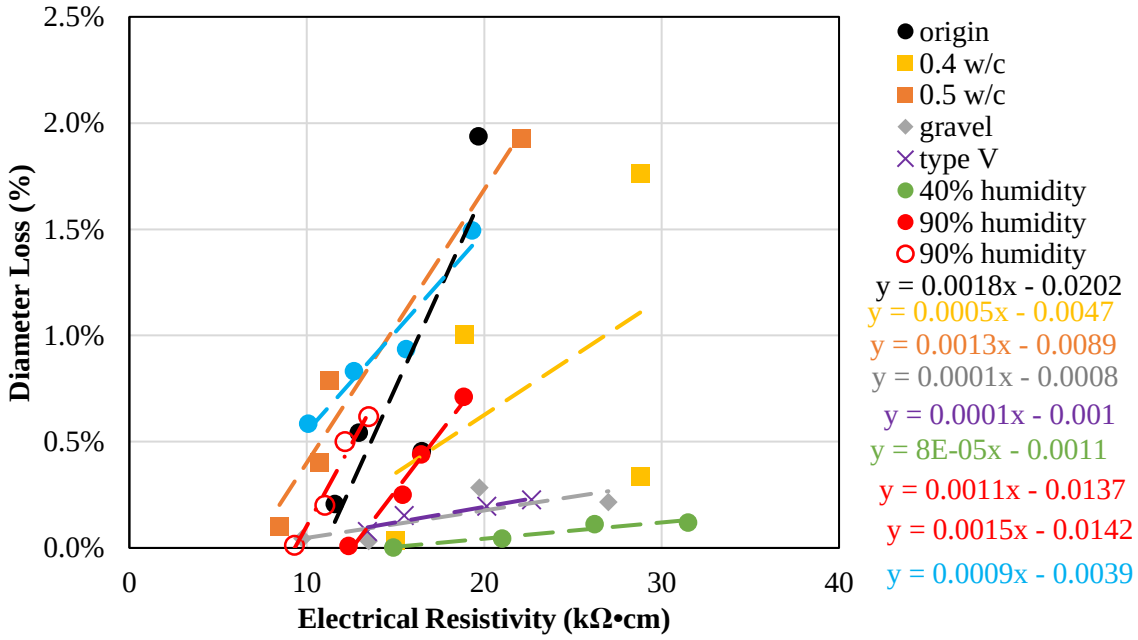

(a) Concrete Prisms submerged in Tap Water or Set inside Humidity Chamber

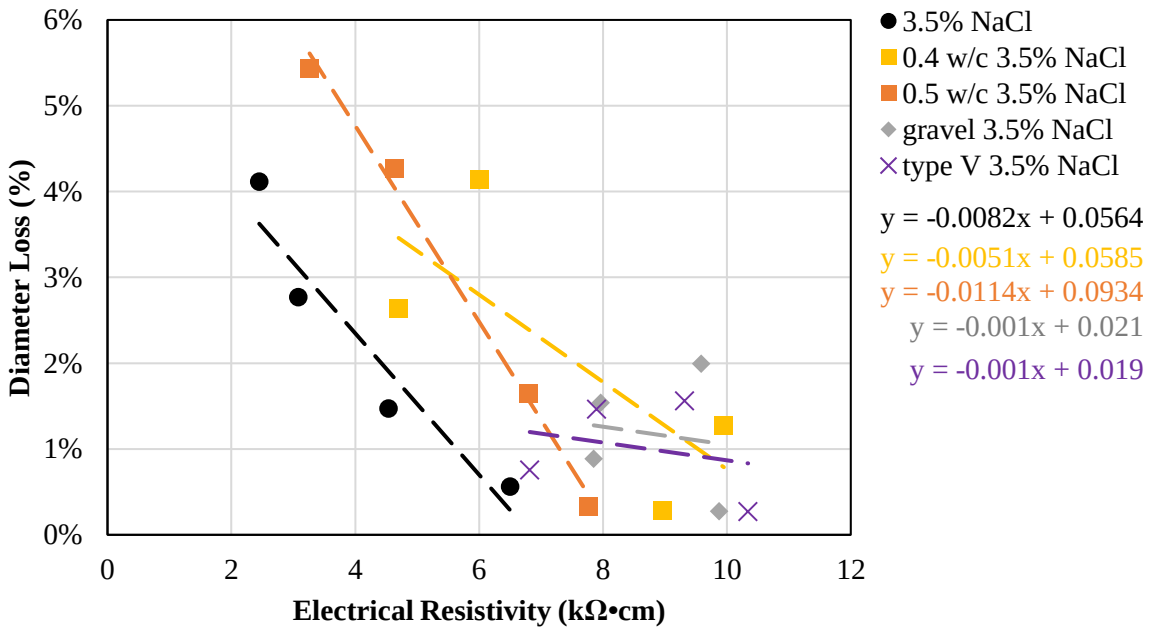

(b) Concrete Prisms Submerged in 3.5% NaCl Solution

Figure 4.17 Correlation of Concrete's Resistivity to the Reinforcement's Diameter Loss

Chapter 5. Closure

5.1 Summary

This study investigated the corrosion rate of the carbon steel reinforcement embedded in concrete and the surface resistivity of the concrete. The test concept, experimental approach and instrumentation used for this accelerated corrosion study are explained in Chapter 3. The results obtained in this study were analyzed in Chapter 4. Lastly, this chapter summarizes the conclusions and other contributions of other corrosion related studies. This chapter also covers recommendations for future research.

5.2 Conclusions

The following conclusions were drawn from the corrosion study:

- The amount of water absorbed by the concrete affects the electrical resistivity readings.
- For concrete submerged in tap water, the resistivity and corrosion rate exhibited a proportional correlation.
- Corrosion rates and resistivity readings had an inverse correlation for concrete submerged or mixed with sodium chloride solution.
- When a concrete prism was disconnected from the amperage and removed from environment, the resistivity readings began to increase steeply, and corrosion rates began to stabilize.
- Highest corrosion rates recorded were distinguished for those concrete specimens under sodium chloride fluids. Highest concrete resistivity was obtained for those specimens in an environmental chamber with low humidity of 40%.
- At day 7 of testing, the resistivity values decreased, corrosion rates gradually increased, and cracking of the specimen was seen for specimens submerged in the chloride content fluid.

- Tafel tests were time consuming and problematic especially in day zero when specimen was moist.
- The corrosion rates measured by LPR were less than those observed experimentally because LPR is not sensitive to nonconductive rust layers.
- LPR coupled with Tafel slopes distinguished the most corrosive environments with higher corrosion rates when compared to the actual diameter loss.
- Corrosion rates decreased by reducing the water cement ratio, using Type V cement, and avoiding the use of contaminated water in the mix.

5.3 Recommendation for Future Work

Since LPR and Tafel only registered some of the oxides and resulted in low corrosion rates, it is necessary to establish a methodology that defines with a high accuracy the level a representative value of corrosion rate of the reinforcement in certain environments with a combination of different electrochemical techniques and to reach reliable status to monitor and assess the corrosion of the reinforcement continuously and accurately with time.

References

1. Angst, U. (2011). Chloride induced reinforcement corrosion in concrete (Unpublished master's thesis). Norwegian University of Science and Technology.

2. Böhni, H. (2005). Corrosion in reinforced concrete structures (1st ed.). Woodhead Publishing Limited.

3. Fakhri, H. (2019, May 17). Corrosion mitigation in reinforced concrete structures using engineered cementitious composites. Retrieved from https://ubir.buffalo.edu/xmlui/handle/10477/80014

4. Fattah, A. A., Al-Duais, I., Riding, K., & Thomas, M. (2018). Field evaluation of corrosion mitigation on reinforced concrete in marine exposure conditions. Construction and Building Materials, 165, 663-674. doi:10.1016/j.conbuildmat.2018.01.077

5. Figueira, R. (2017). Electrochemical Sensors for Monitoring the Corrosion Conditions of Reinforced Concrete Structures: A Review. Applied Sciences, 7(11), 1157. doi:10.3390/app7111157

6. Gucunski, N., Imani, A., Romero, F., Nazarian, S., Yuan, D., Wiggenhauser, H., . . . Kutrubes, D. (2013). Nondestructive testing to identify concrete bridge deck deterioration (pp. 1-83, Publication No. S2-R06A-RR-1). Washington D.C.: Transportation Research Board.

7. Hœrlé, S., Mazaudier, F., Dillmann, P., & Santarini, G. (2004). Advances in understanding atmospheric corrosion of iron. II. Mechanistic modelling of wet–dry cycles. Corrosion Science, 46(6), 1431-1465. doi:10.1016/j.corsci.2003.09.028

8. Hornbostel, K., Larsen, C. K., & Geiker, M. R. (2013). Relationship between concrete resistivity and corrosion rate – A literature review. Cement and Concrete Composites, 39, 60-72. doi:10.1016/j.cemconcomp.2013.03.019

9. Lau, K., & Zhou, L. (2001, September 7). Mechanical performance of composite-strengthened concrete structures. Composites Part B: Engineering, 32(1), 21-31. doi:10.1016/s1359-8368(00)00043-3

10. Liu, Y., & Weyers, R. E. (1998). Modeling the time-to-corrosion cracking in chloride contaminated reinforced concrete structures. ACI Materials Journal, 95(6), 675-681.

11. Loukil, O., Adelaide, L., Bouteiller, V., Quiertant, M., Chaussadent, T., Ragueneau, F., . . . Trenty, L. (Aug. 2016). Experimental study of corrosion-induced degradation of reinforced concrete elements. International RILEM Conference on Materials, Systems and Structures in Civil Engineering Conference Segment on Electrochemistry in Civil Engineering.

12. Polder, R. B. (2001, February 1). Test methods for on-site measurement of resistivity of concrete — a RILEM TC-154 technical recommendation. Construction and Building Materials, 15(2-3), 125-131. doi:10.1016/s0950-0618(00)00061-1

13. Pradityana, A., Sulistijono, Shahab, A., Noerochim, L., & Susanti, D. (2016, August 31). Inhibition of Corrosion of Carbon Steel in 3.5% NaCl Solution by Myrmecodia Pendans Extract. Retrieved from https://www.hindawi.com/journals/ijc/2016/6058286/

14. Silva, M., Cunha, M., Pinho-Ramos, A., Sena da Fonseca, B., & Pinho, F. (2017). Accelerated action of external sulfate and chloride to study corrosion of tensile steel in reinforced concrete. Materiales de Construcción, 67(328), e141. doi:http://dx.doi.org/10.3989/mc.2017.10116

15. Suryavanshi, A., Scantlebury, J., & Lyon, S. (1998, September 22). Corrosion of reinforcement steel embedded in high water-cement ratio concrete contaminated with chloride. Cement and Concrete Composites, 20(4), 263-281. doi:10.1016/s0958-9465(98)00018-3

16. Tuutti, K. (1982). Corrosion of steel in concrete. Swedish Cement and Concrete Research Institute, Stockholm

17. Xiao, J., Qu, W., Li, W., & Zhu, P. (2016). Investigation on effect of aggregate on three non-destructive testing properties of concrete subjected to sulfuric acid attack. Construction and Building Materials, 115, 486-495. doi:10.1016/j.conbuildmat.2016.04.017

18. Yang, E., & Zhang, G. (2016). Polarization resistance of steel bar embedded in engineered cementitious composite under direct current exertion. International RILEM Conference Materials Systems, 141-149.

19. Zhang, J., & Cheung, M. M. (2012). Modeling of chloride-induced corrosion in reinforced concrete structures. Materials and Structures, 46(4), 573-586. doi:10.1617/s11527-012-9914-2

Vita

Luisa Alejandra Morales was born and raised in El Paso Texas. Her interest in engineering flickered when she was young as she spent most of her time with her father and grandfather, Ismael Morales and Alfonso Reynoso. In admiration of her father and grandfather, she was motivated to pursue a career in construction. She graduated from Coronado High School in 2012 and begin to study Civil Engineering in The University of Texas at El Paso. In 2018, she received her Bachelor's in Civil Engineering in 2018 and afterwards pursued in earning a degree in Master of Science in Civil Engineering.

In her junior year, she was admitted as a volunteer research assistant at The Center for Transportation Infrastructure Systems (CTIS). She began working with a project of studying soil resistance with machinery and later moved to help on a bigger project were she performed research on saturated soil resistance and galvanized steel for mechanically stabilized earth (MSE) walls, under the guidance of Dr. Soheil Nazarian and Dr. Arturo Bronson. CTIS gave her two whole years of knowledge and experience due to the projects that she had a chance to participate. The past two years, Dr. Nazarian gave her the opportunity to begin on a new part of the past research project which was her thesis for her master's degree in Civil Engineering.

Since 2016, Luisa had the opportunity to be part of the Transportation Leadership Council (TLC) UTEP Chapter. TLC is a student organization founded by the Southern Plains Transportation Center. Now that she has obtained my master's degree in civil engineering with the help of the center and her mentors she would like to keep participating on research meetings and network with professional engineers. Her education will help her pursue her career goals, improve, and reinforce our state's infrastructures systems.